L3

Dinamica e identificazione di processi forzati non stazionari

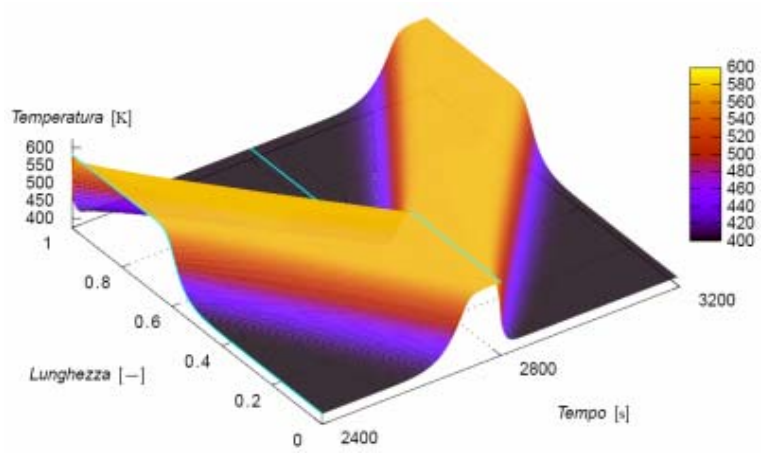

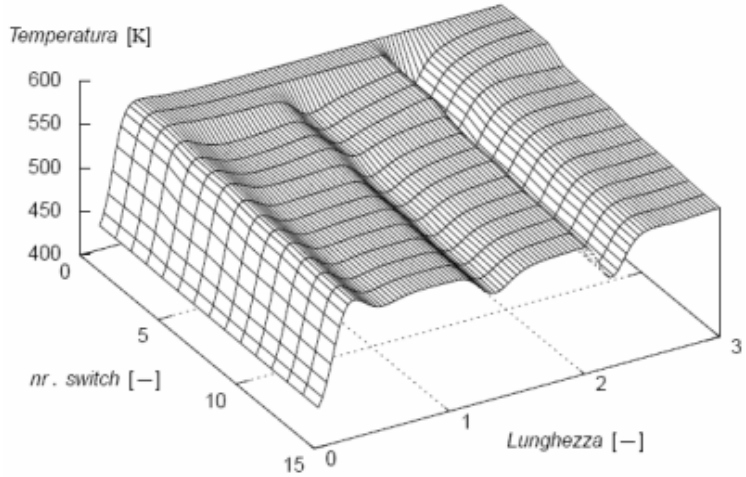

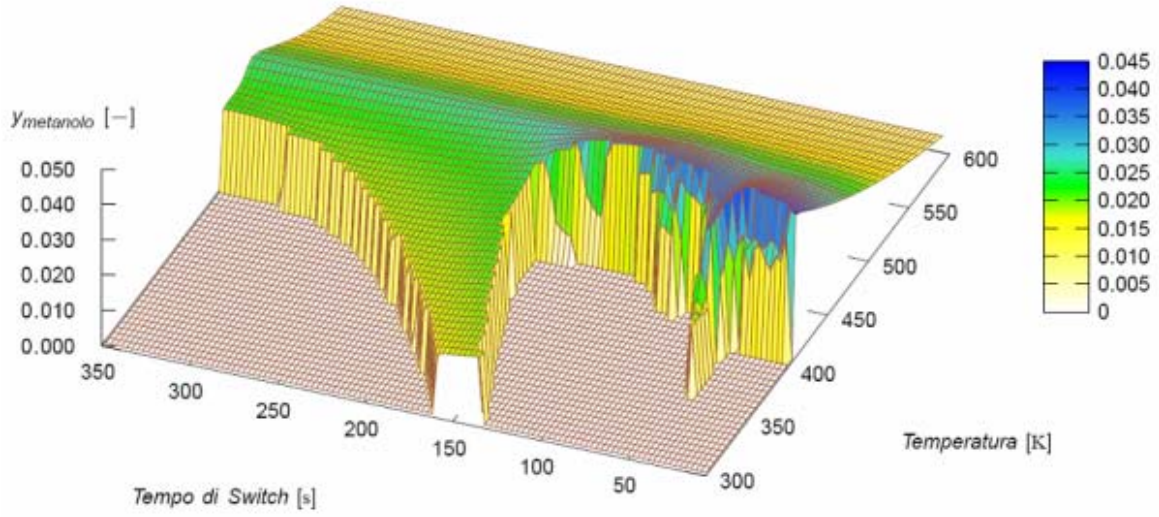

Forced unsteady state reactors

- Forced unsteady state reactors allow reaching higher conversions than conventional reactors.
- Two alternatives:
  - Reverse flow reactors, **RFR**;
  - Network of reactors: simulated moving bed reactors, **SMBR**.
- Within a **SMBR** network, the simulated moving bed is accomplished by periodically switching the feed inlet from one reactor to the following one.
- **APPLICATION**: Methanol synthesis (ICI patent).
  - Operating temperature: 220-300 °C;
  - Pressure: 5-8 MPa;
  - CO = 10-20%; CO_2 = 6-10%; H_2 = 70-80%.

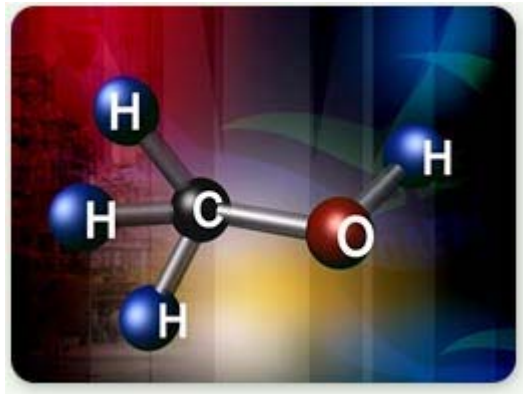

Forced unsteady state reactors

- Conduzione di reazioni catalitiche esotermiche in modo autotermico.
- Utilizzo vantaggioso soprattutto quando la concentrazione dei reagenti o l'esotermia della/delle reazioni sono basse.
- Incremento di conversione e di produttività che consente:
  - l'utilizzo di reattori più piccoli,
  - minore quantità di catalizzatori.

Sintesi del metanolo in reattori non stazionari forzati

- La reazione di sintesi del metanolo è la seguente:

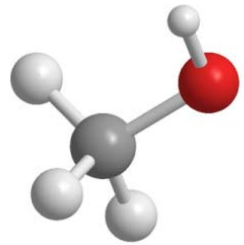

$$CO + 2H_2 \rightleftarrows CH_3OH \qquad \Delta\tilde{H}_R = -90.769 \text{ kJ/mol}$$

- La reazione avviene con diminuzione del numero di moli, quindi si lavora ad alte pressioni.
- I primi impianti lavoravano a circa 100 ÷ 600 atm.
- Gli impianti attuali lavorano a pressioni inferiori (50 – 80 atm).
- Negli impianti a bassa pressione sono significative anche le seguenti reazioni:

$$CO_2 + H_2 \rightleftarrows CO + H_2O$$
$$CO_2 + 3H_2 \rightleftarrows CH_3OH + H_2O$$

Reverse Flow Reactors

- Il sistema di valvole V_1, V_2, V_3, V_4 permette l'inversione periodica della corrente di alimentazione.

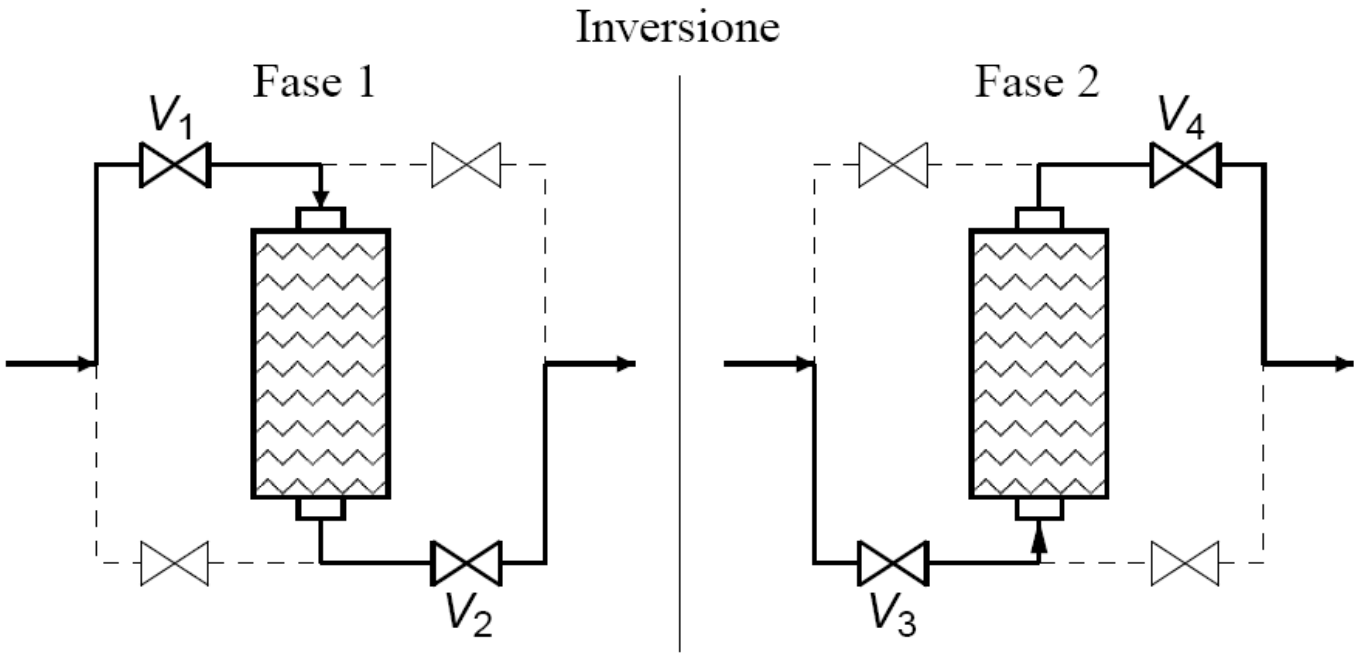

RFR: modello basato su principi primi

Equazioni	N° eq.	Tipo eq.	Variabili
Bilancio entalpico fase gas	1	derivate parziali	$T_G, T_S, \underbrace{y_{G,i}}_{\text{i=1...nComp}}$
Bilancio entalpico fase solida (catalizzatore)	1	derivate parziali	$T_G, T_S, \underbrace{y_{G,i}}_{\text{i=1...nComp}}, \underbrace{y_{S,i}}_{\text{i=1...nComp}}$
Bilancio di materia fase gas	nComp	derivate parziali	$T_G, T_S, \underbrace{y_{G,i}}_{\text{i=1...nComp}}, \underbrace{y_{S,i}}_{\text{i=1...nComp}}$
Bilancio di materia fase solida (catalizzatore)	nComp	algebriche non lineari	$T_G, T_S, \underbrace{y_{G,i}}_{\text{i=1...nComp}}, \underbrace{y_{S,i}}_{\text{i=1...nComp}}$

$2\,nComp + 2$ $\qquad$ $2\,nComp + 2$

RFR: sintesi del metanolo

Diametro reattore	D_R	0.1	[m]
Lunghezza	L	0.5	[m]
Grado di vuoto	ϵ	0.4	[–]
Massa catalizzatore	W	41.2	[kg]
Densità apparente catalizzatore	ρ_S	1750	[kg/m^3]
Porosità catalizzatore	ϵ_S	0.5	[–]
Diametro pellet	d_p	0.0054	[m]
Temperatura di alimentazione	T_{in}	373.15	[K]
Pressione di esercizio	P	5	[MPa]
Portata superficiale	F_{in}	32.65	[mol/m^2/s]

RFR: sintesi del metanolo

Specie nel gas in ingresso	Frazione molare
CO	0.045
CO_2	0.02
H_2	0.935

Tipologia catalizzatore	$Cu/Zn/Al_2O_3$ oppure $Cu/Zn/Cr_2O_3$
Contenuto di CuO	$50\% \div 70\%$
Contenuto di ZnO	$20\% \div 30\%$
Durata	circa 2 anni
Cause disattivazione	presenza di zolfo sinterizzazione Cu ($T > 573\,\mathrm{K}$)

Reverse Flow Reactors

- Profilo di temperatura una volta raggiunta la condizione di pseudo-stazionarietà.

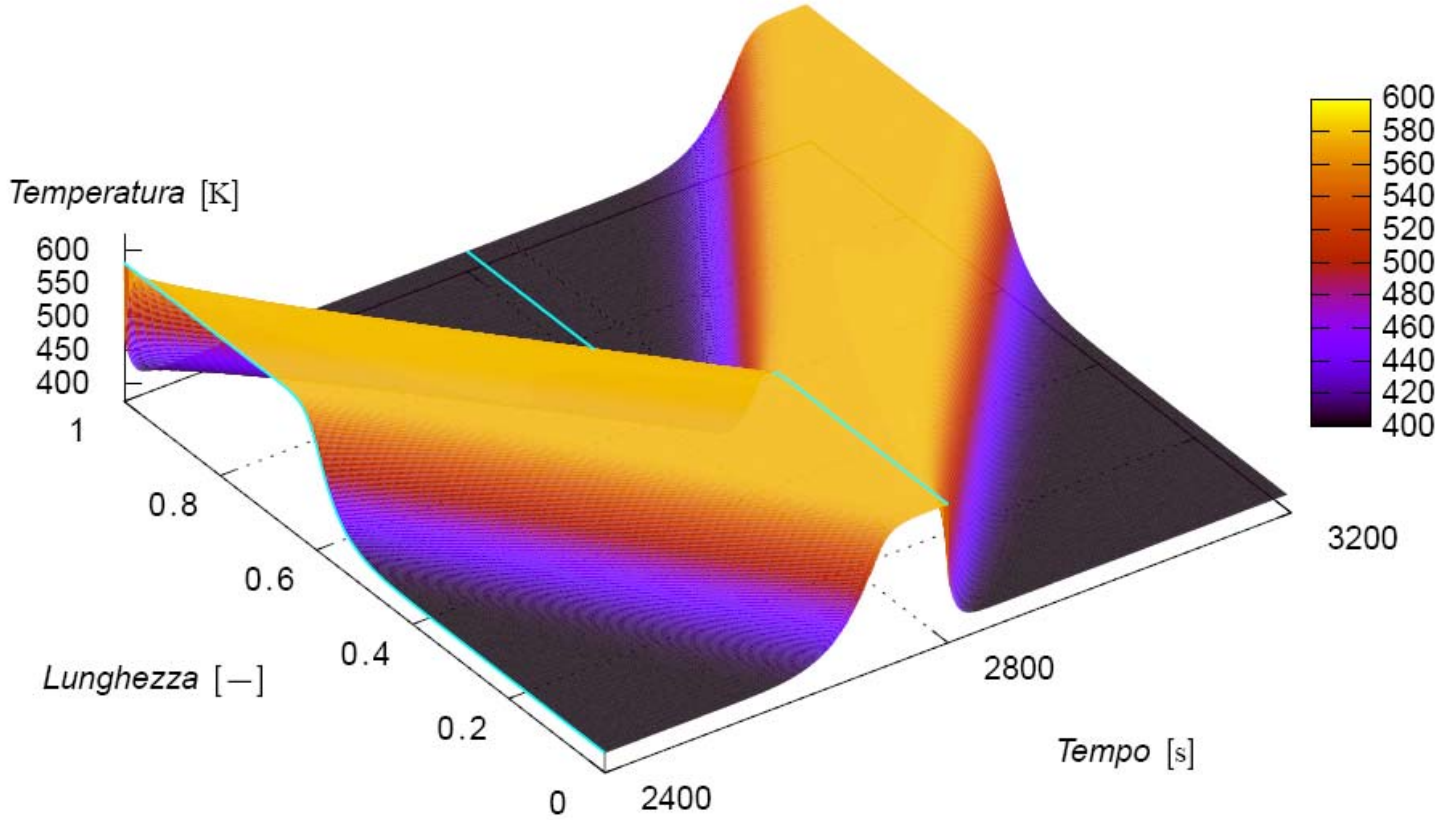

Reverse Flow Reactors

- Profilo di concentrazione del prodotto una volta raggiunta la condizione di pseudo-stazionarietà.

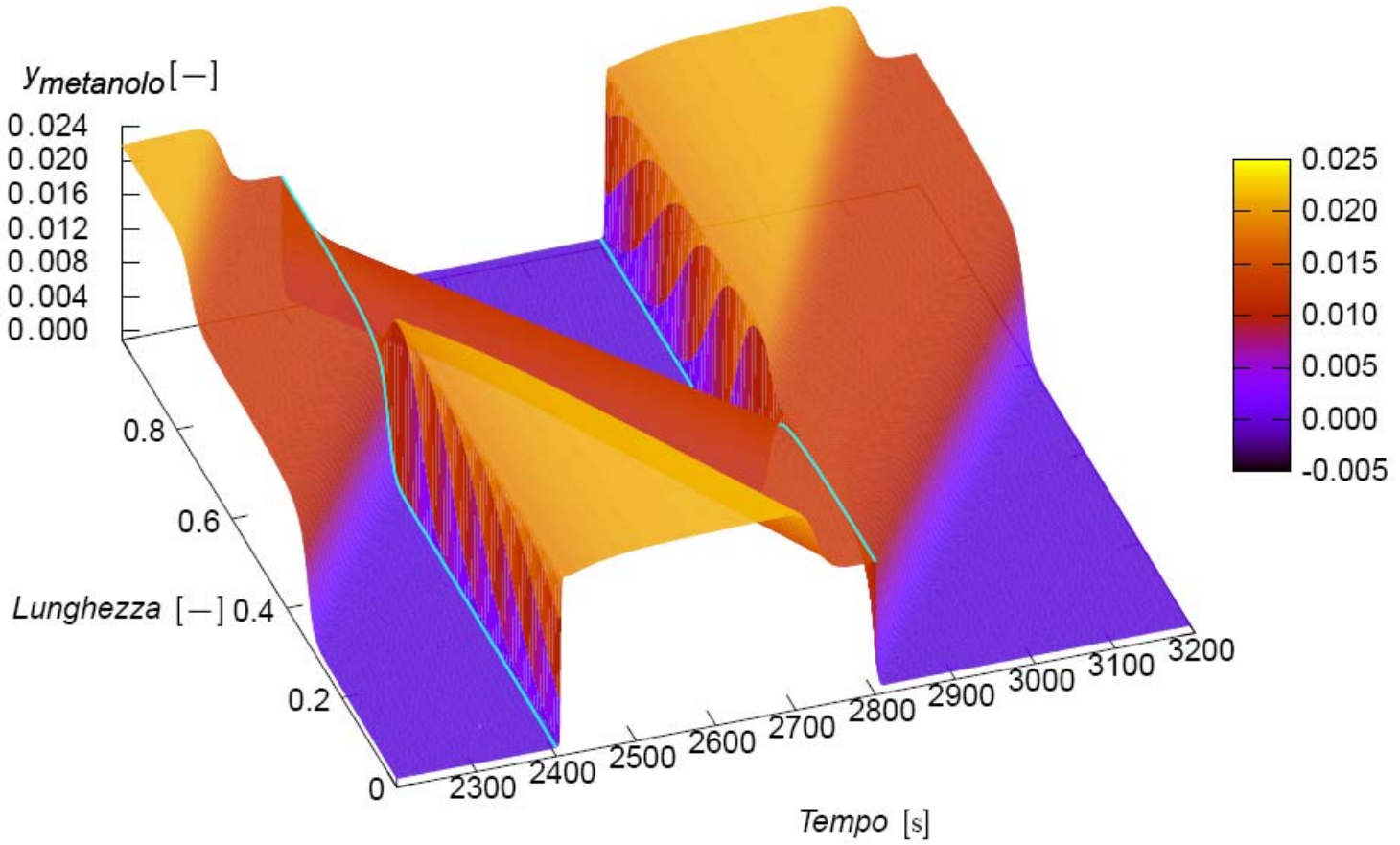

Simulated Moving Bed Reactors

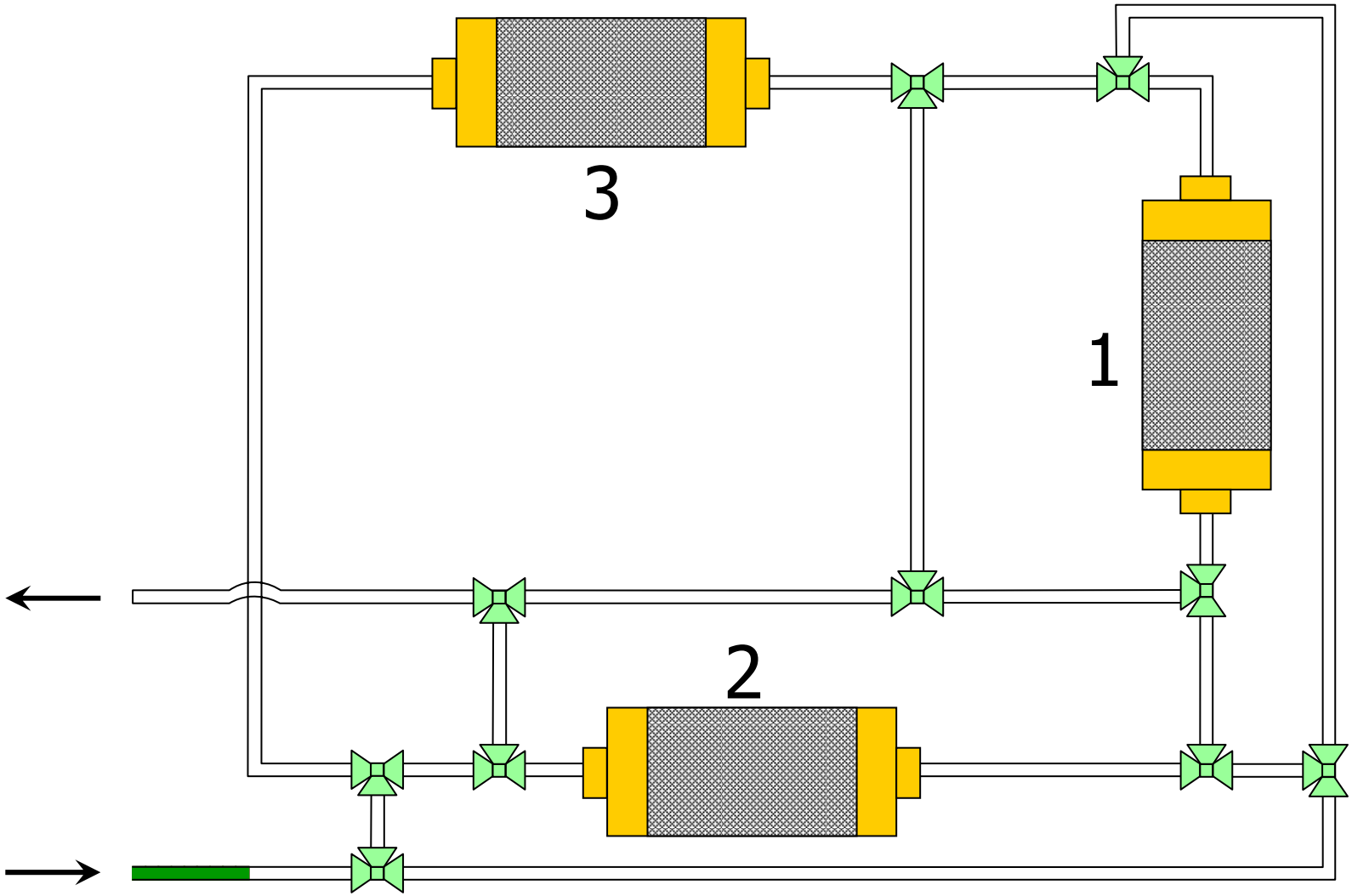

Step 3: 3→1→2

Simulated Moving Bed Reactors

Velardi S., A. Barresi, D. Manca, D. Fissore, Chem. Eng. J., 99 117–123, 2004

- Continuity equation for the gas phase:

$$\frac{\partial c_G}{\partial t} + \frac{\partial}{\partial x} c_G v = \sum_{i=1}^{n_r} \frac{k_{G,i} a_v}{\varepsilon} (y_{S,i} - y_{G,i}). \quad (1)$$

- Continuity equation for component j in the gas phase:

$$\frac{\partial y_{G,j}}{\partial t} = D_{eff} \frac{\partial^2 y_{G,j}}{\partial x^2} - v \frac{\partial y_{G,j}}{\partial x} + \frac{k_{G,j} a_v}{c_G \varepsilon} (y_{S,j} - y_{G,j}) - y_{G,j} \sum_{i=1}^{n_r} \frac{k_{G,i} a_v}{c_G \varepsilon} (y_{S,i} - y_{G,i})$$

$$\text{with } j = 1, \ldots, (n_r - 1). \quad (2)$$

- Energy balance for the gas phase:

$$\frac{\partial T_G}{\partial t} = \frac{k_{eff}}{\varrho \hat{c}_{P,G}} \frac{\partial^2 T_G}{\partial x^2} - v \frac{\partial T_G}{\partial x} + \frac{h a_v}{\varrho \hat{c}_{P,G} \varepsilon} (T_S - T_G). \quad (3)$$

- Mass balance for the solid phase:

$$k_{G,j} a_v (y_{S,j} - y_{G,j}) = [\varrho_S (1 - \varepsilon)] \sum_{k=1}^{N_R} \eta_k \nu_{j,k} R'_k$$

$$\text{with } j = 1, \ldots, n_r. \quad (4)$$

- Energy balance for the solid phase:

$$\frac{\partial T_S}{\partial t} = \frac{\lambda_S}{\varrho_S \hat{c}_{P,S}} \frac{\partial^2 T_S}{\partial x^2} - \frac{h a_v}{\varrho_S \hat{c}_{P,S} (1 - \varepsilon)} (T_S - T_G) + \frac{1}{\hat{c}_{P,S}} \sum_{i=1}^{n_r} \left(\sum_{k=1}^{N_R} \eta_k \nu_{i,k} R'_k \right) (-\Delta \tilde{H}_{f,i}). \quad (5)$$

• Kinetic equations corresponding to a dual-site Langmuir-Hinshelwood mechanism, based on three independent reactions: methanol formation from CO, water-gas-shift reaction and methanol formation from CO2:

$$CO + 2H_2 \rightleftharpoons CH_3OH, \quad (6)$$

$$CO_2 + H_2 \rightleftharpoons CO + H_2O, \quad (7)$$

$$CO_2 + 3H_2 \rightleftharpoons CH_3OH + H_2O. \quad (8)$$

Simulated Moving Bed Reactors

Velardi S., A. Barresi, D. Manca, D. Fissore, Chem. Eng. J., 99 117–123, 2004

• Reaction rates for a catalyst based on Cu–Zn–Al mixed oxides

$$R'_{CH_3OH,A} = \frac{k'_{ps,A} K_{CO} \left[p_{CO} p_{H_2}^{3/2} - \frac{p_{CH_3OH}}{p_{H_2}^{1/2} K_{p,A}} \right]}{(1 + K_{CO} p_{CO} + K_{CO_2} p_{CO_2})[p_{H_2}^{1/2} + (K_{H_2O}/K_{H_2}^{1/2}) p_{H_2O}]}, \quad (9)$$

$$R'_{H_2O,B} = \frac{k'_{ps,B} K_{CO_2} \left[p_{CO_2} p_{H_2} - \frac{p_{H_2O} p_{CO}}{K_{p,B}} \right]}{(1 + K_{CO} p_{CO} + K_{CO_2} p_{CO_2})[p_{H_2}^{1/2} + (K_{H_2O}/K_{H_2}^{1/2}) p_{H_2O}]}, \quad (10)$$

$$R'_{CH_3OH,C} = R'_{H_2O,C} = \frac{k'_{ps,C} K_{CO_2} \left[p_{CO_2} p_{H_2}^{3/2} - \frac{p_{CH_3OH} p_{H_2O}}{(p_{H_2}^{3/2} K_{p,C})} \right]}{(1 + K_{CO} p_{CO} + K_{CO_2} p_{CO_2})[p_{H_2}^{1/2} + (K_{H_2O}/K_{H_2}^{1/2}) p_{H_2O}]}. \quad (11)$$

Concerning the gas-solid heat transfer coefficient, the following correlation has been adopted:

$$\frac{h d_P}{\lambda_G} = 1.6(2 + F Re_P^{0.5} Pr^{1/3}) \quad (12)$$

with

$$F = 0.664 \sqrt{1 + \left[\frac{0.0557 Re_P^{0.3} Pr^{2/3}}{1 + 2.44(Pr^{2/3} - 1) Re_P^{-0.1}} \right]^2} \quad (13)$$

Simulated Moving Bed Reactors

Velardi S., A. Barresi, D. Manca, D. Fissore, Chem. Eng. J., 99 117–123, 2004

The prediction of the axial heat dispersion coefficient has been carried out adopting a correlation by Dixon and Cresswell [15]:

$$\frac{k_{\text{eff}}}{\varrho v \hat{c}_{P,\text{G}} d_{\text{P}}} = \frac{0.73 + (\lambda_{\text{st}}/\lambda_{\text{G}})}{Re_{\text{P}} Pr} + \frac{0.5}{1 + 9.7(Re_{\text{P}} Pr)}, \qquad (14)$$

where the term $\lambda_{\text{st}}/\lambda_{\text{G}}$ accounts for the stagnant zone contribution. According to Edwards and Richardson [16] a correlation of the same general form as Eq. (14) can be used for the prediction of mass dispersion coefficient:

$$\frac{D_{\text{eff}}}{v d_{\text{P}}} = \frac{0.73}{Re_{\text{P}} Sc} + \frac{0.5}{1 + 9.7/(Re_{\text{P}} Sc)}. \qquad (15)$$

Conventional Danckwerts boundary conditions are assumed at the inlet section of the network. The continuity of the gas temperature and concentration profiles has been imposed between each reactor of the sequence, at sections $x = \ell$ and 2ℓ. In addition, spatial derivatives should vanish at the outlet sections. At time $t = 0$ the reactants concentration is null, while the initial temperatures of the gas and solid phases are the same. When the switching time is reached the origin of the x-axis moves from the first reactor of the sequence to the second one and the switching conditions are applied in order to simulate the change of the inlet position:

$$x \in]0, 2\ell[\quad \begin{cases} y_{\text{G},j}(x)|_{t+} = y_{\text{G},j}(x+\ell)|_{t-} \\ T_{\text{G}}(x)|_{t+} = T_{\text{G}}(x+\ell)|_{t-} \\ T_{\text{S}}(x)|_{t+} = T_{\text{S}}(x+\ell)|_{t-} \end{cases},$$

$$x \in [2\ell, 3\ell] \quad \begin{cases} y_{\text{G},j}(x)|_{t+} = y_{\text{G},j}(x-2\ell)|_{t-} \\ T_{\text{G}}(x)|_{t+} = T_{\text{G}}(x-2\ell)|_{t-} \\ T_{\text{S}}(x)|_{t+} = T_{\text{S}}(x-2\ell)|_{t-} \end{cases}. \qquad (16)$$

Simulated Moving Bed Reactors

- Dopo un numero sufficiente di switch il profilo di temperatura assume una conformazione **pseudo-stazionaria**.

Alti tempi di switch

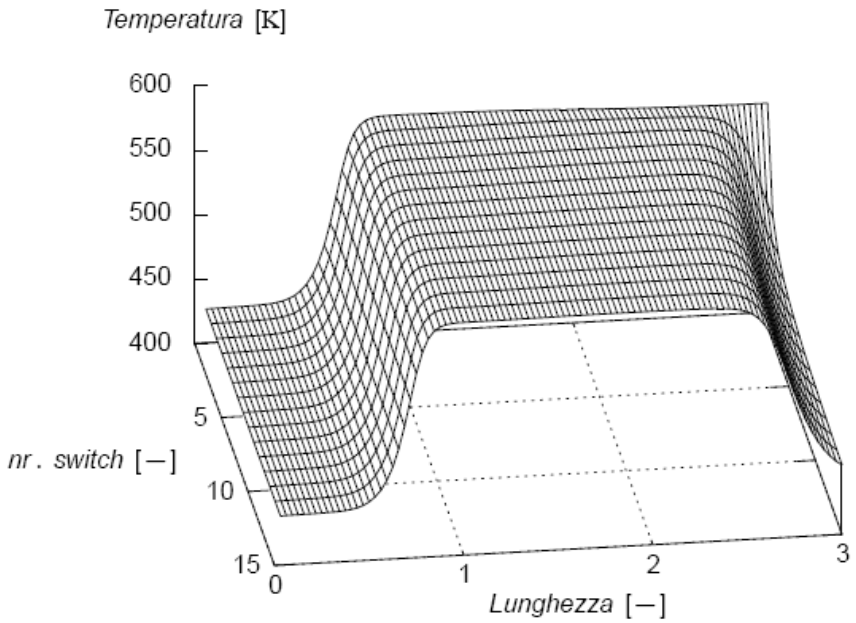

Bassi tempi di switch

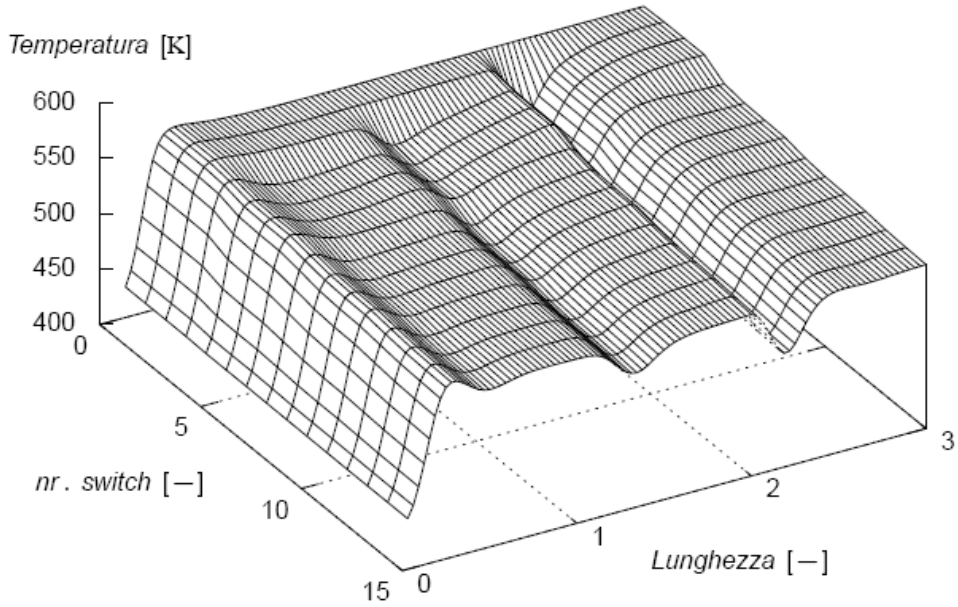

SMBR: the thermal wave

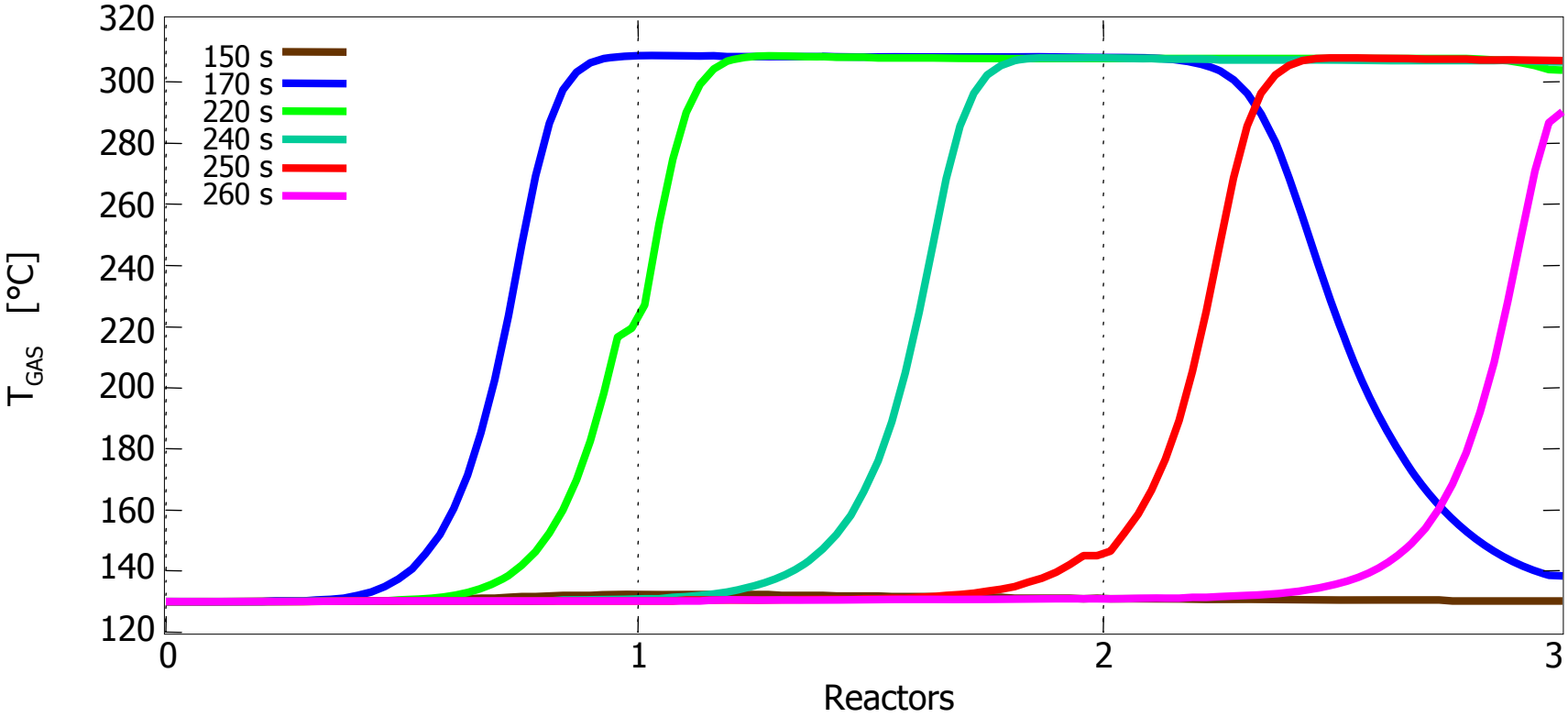

SMBR: risposta ad anello aperto

Velardi S., A. Barresi, D. Manca, D. Fissore, Chem. Eng. J., 99 117–123, 2004

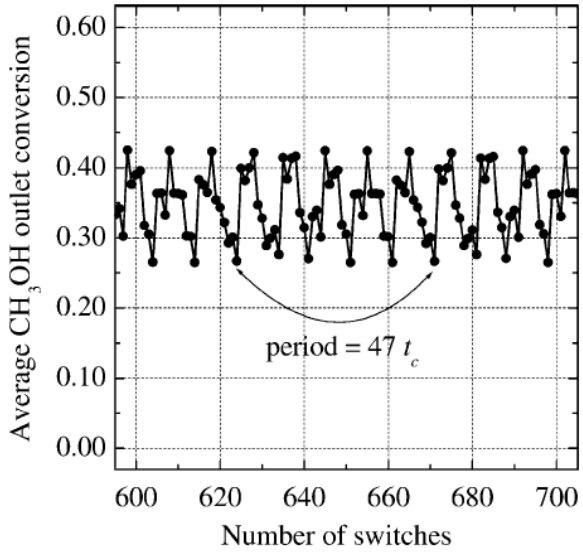

Fig. 5. Periodic evolution of the average methanol outlet conversion in the complex behaviour region; $t_c = 20$ s, $T_{in} = 100$ °C.

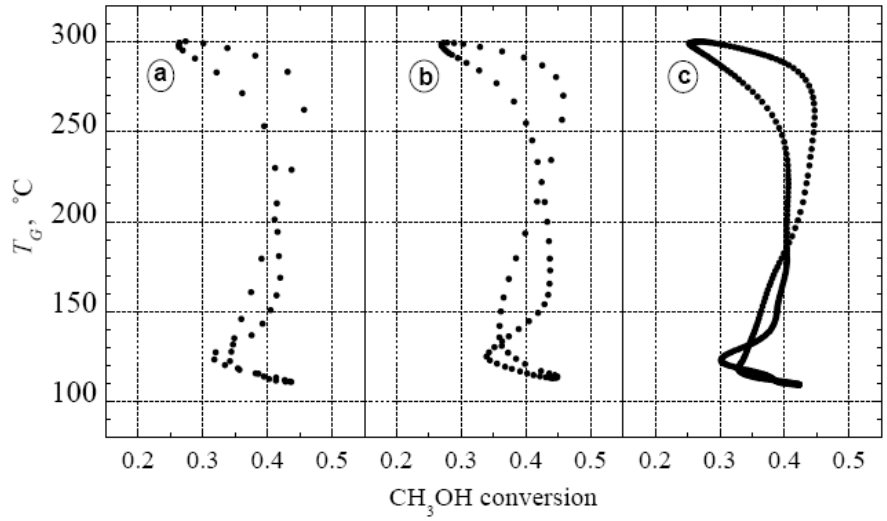

Fig. 6. Correlation between methanol conversion and the outlet gas temperature for different switching times. (a) Period = $47t_c$, $t_c = 20$ s; (b) period = $72t_c$, $t_c = 22$ s; (c) period = $332\,t_c$, $t_c = 24$ s. Points are taken in the middle of each cycle.

SMBR: risposta ad anello aperto

Velardi S., A. Barresi, D. Manca, D. Fissore, Chem. Eng. J., 99 117–123, 2004

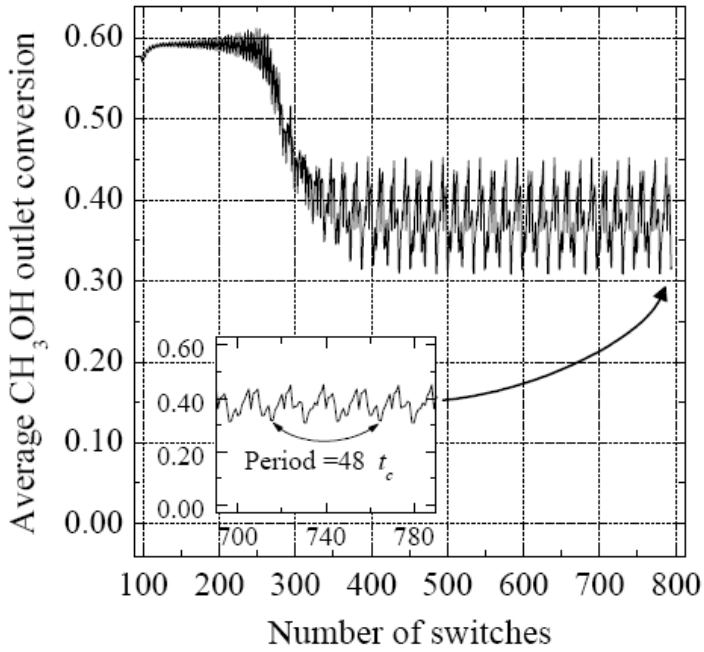

Fig. 7. Open loop response to a step disturbance $\Delta T_{G,in} = -10\,^{\circ}C$ and transition to a multi-periodic steady-state; $t_c = 40\,s$, $T_{in} = 130\,^{\circ}C$.

SMBR: risposta ad anello aperto

Velardi S., A. Barresi, D. Manca, D. Fissore, Chem. Eng. J., 99 117–123, 2004

Stop disturbo dopo **195** cicli

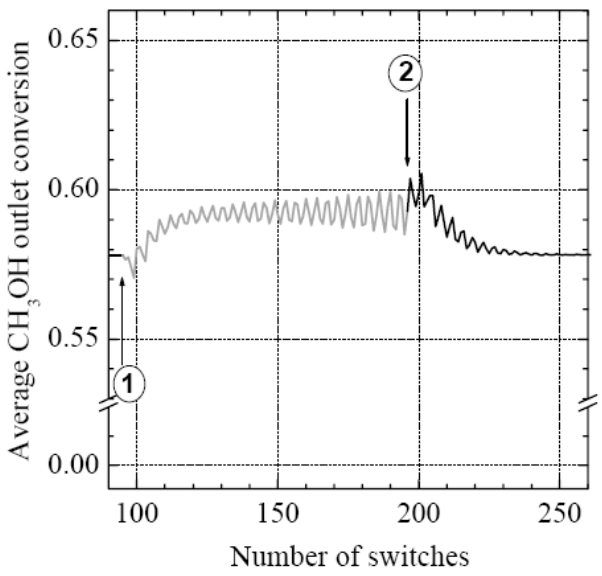

Fig. 8. Open loop response to a step disturbance $\Delta T_{G,in} = -10\,^{\circ}C$ (point 1) and restoration of the previous steady-state after the disturbance (point 2); $t_c = 40\,s$, $T_{in} = 130\,^{\circ}C$.

Stop disturbo dopo **200** cicli

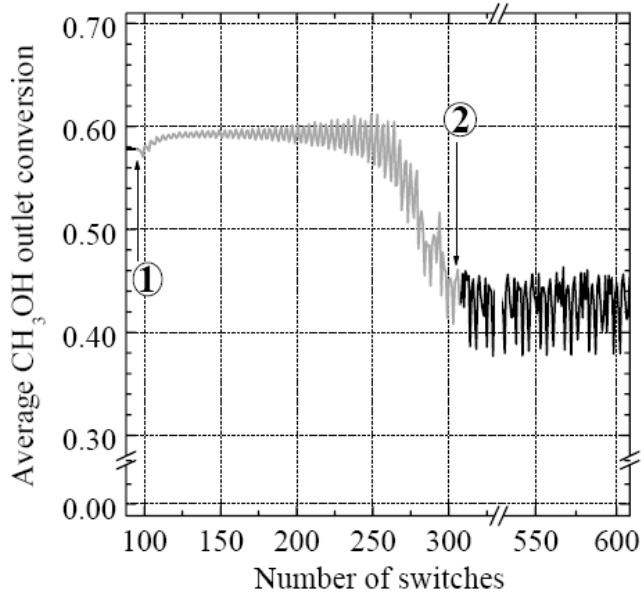

Fig. 9. Open loop response to a step disturbance $\Delta T_{G,in} = -10\,^{\circ}C$ (point 1) and new complex steady-state obtained when the conditions before the disturbance are restored (point 2); $t_c = 40\,s$, $T_{in} = 130\,^{\circ}C$.

Esistenza di più stati stazionari periodici

The control problem

- **FEATURES**
  - The system may suddenly diverge to unstable operating conditions (even chaotic behavior);
  - The network may shut-down;
  - The reactors may work in a suboptimal region.
- **PROBLEM**
  - The reactor network should work within an optimal operating range;
  - Such a range is often narrow and its identification may be difficult.
- **SOLUTION**
  - A suitable control system must be synthesized and implemented on-line to avoid either shut-down or chaotic behaviors;
  - An advanced control system is highly recommend;
  - Model based control → Model Predictive Control, **MPC**.

Numerical modeling

- The model based approach to the control problem calls for the implementation of a **numerical model** of the network that will be used for:
  1. **Identification** of the optimal operating conditions;
  2. **Control purposes**, *i.e.* to predict the future behavior of the system.

- The numerical model is based on a first principles approach:
  - The reactors are continuously evolving (they never reach a steady-state condition) → time derivative;
  - Each PFR reactor must be described spatially → spatial derivative;
  - The reacting system is catalyzed (therefore it is heterogeneous). Consequently, an algebraic term is required → **PDAE system**.
  - The PDAE system is spatially discretized → **DAE system**.
  - A total of **1067 differential and algebraic equations** must be integrated to determine the dynamic evolution of the network.

Accorgimenti matematici...

Chiusura stechiometrica:

$$y_{G,nComp} = 1 - \sum_{iComp=1}^{nComp-1} y_{G,iComp}$$

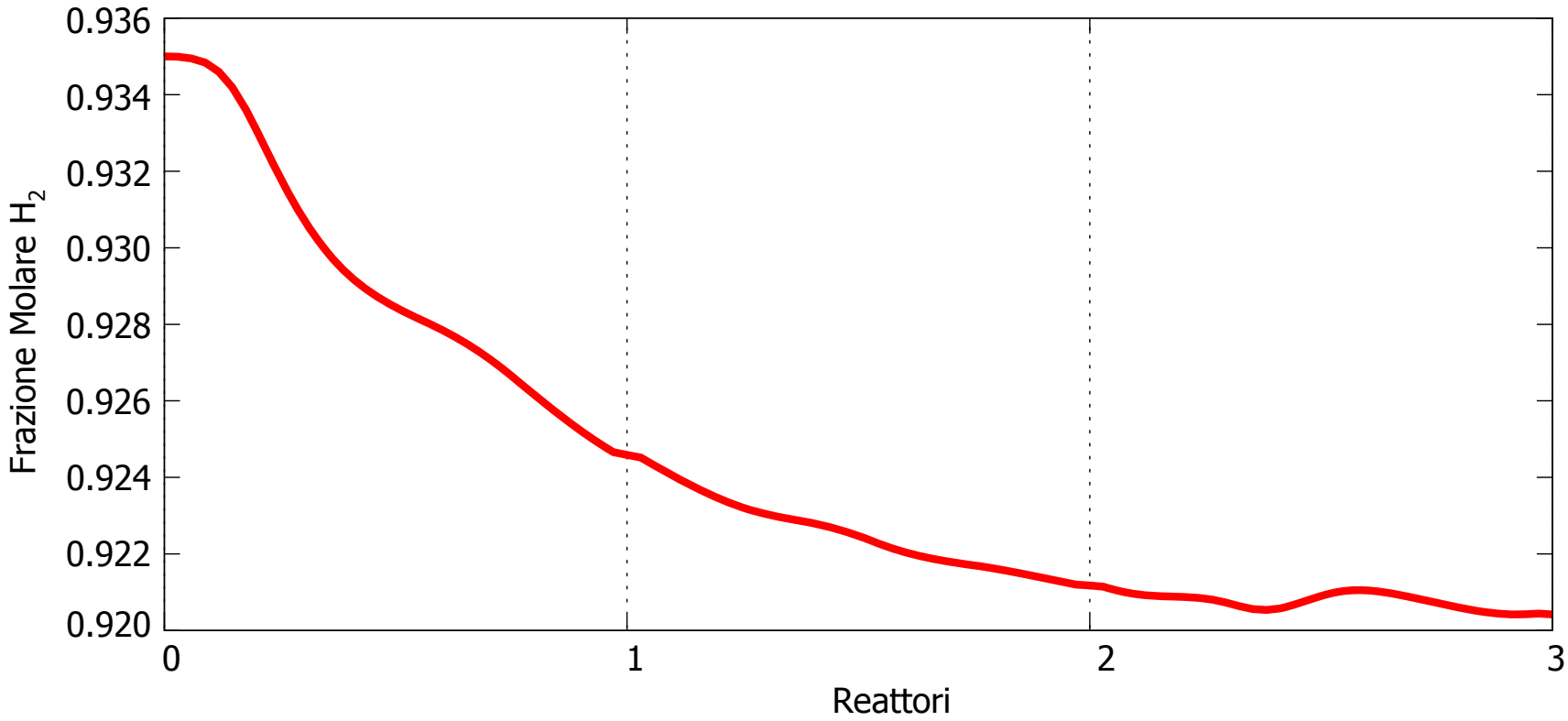

Risoluzione numerica sistema DAE

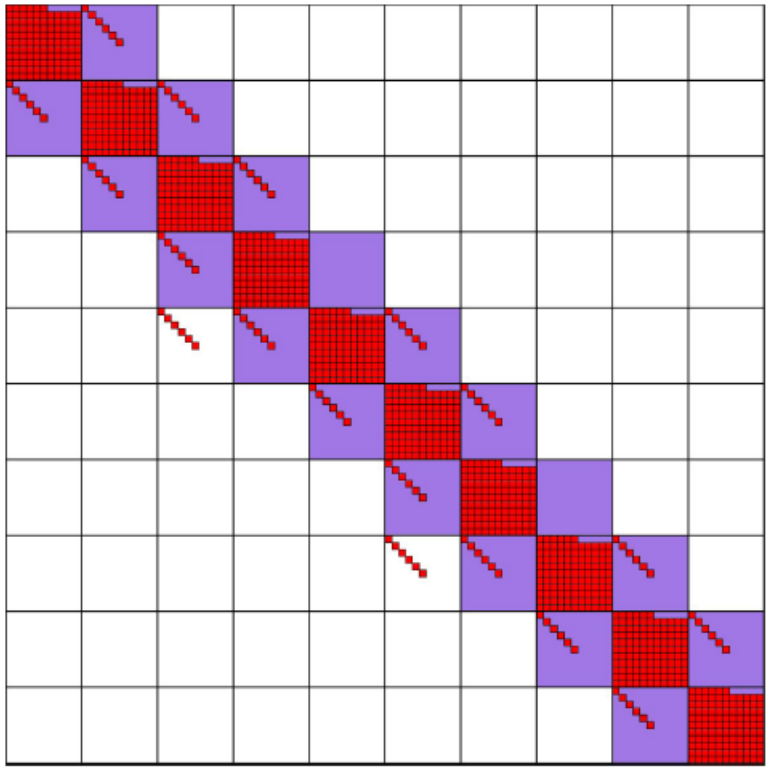

Matrice degli indici di presenza del sistema algebrico-differenziale.

Algoritmo risolutore specifico per:

- sistemi tridiagonali a blocchi (*BzzTridiagonalBlocks*)

Risoluzione numerica sistema DAE

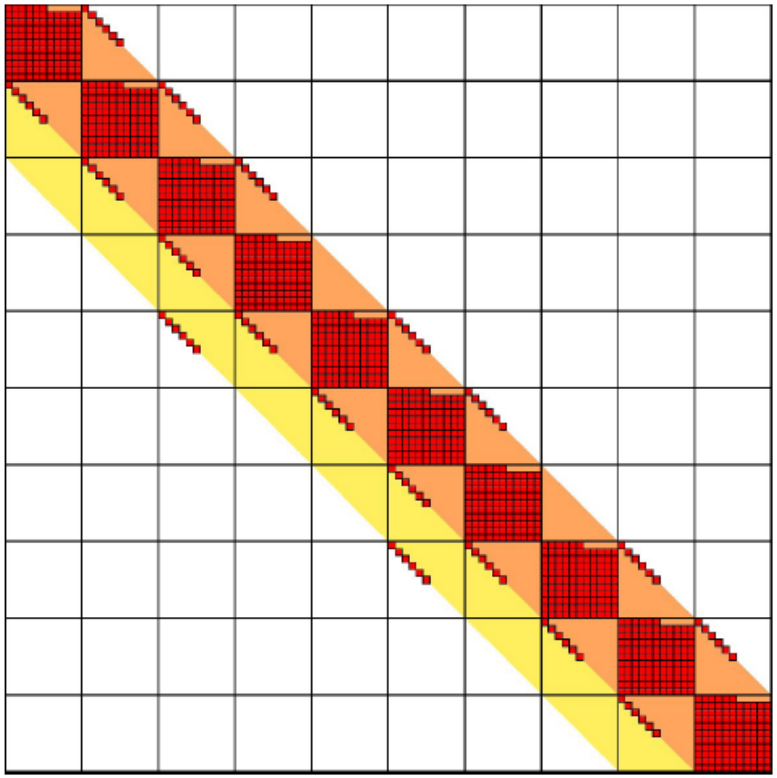

Matrice degli indici di presenza del sistema algebrico-differenziale.

Algoritmo risolutore specifico per:

- sistemi a banda (*BzzDAEBanded*)

Risoluzione numerica sistema DAE

BzzDAEFourBlocks

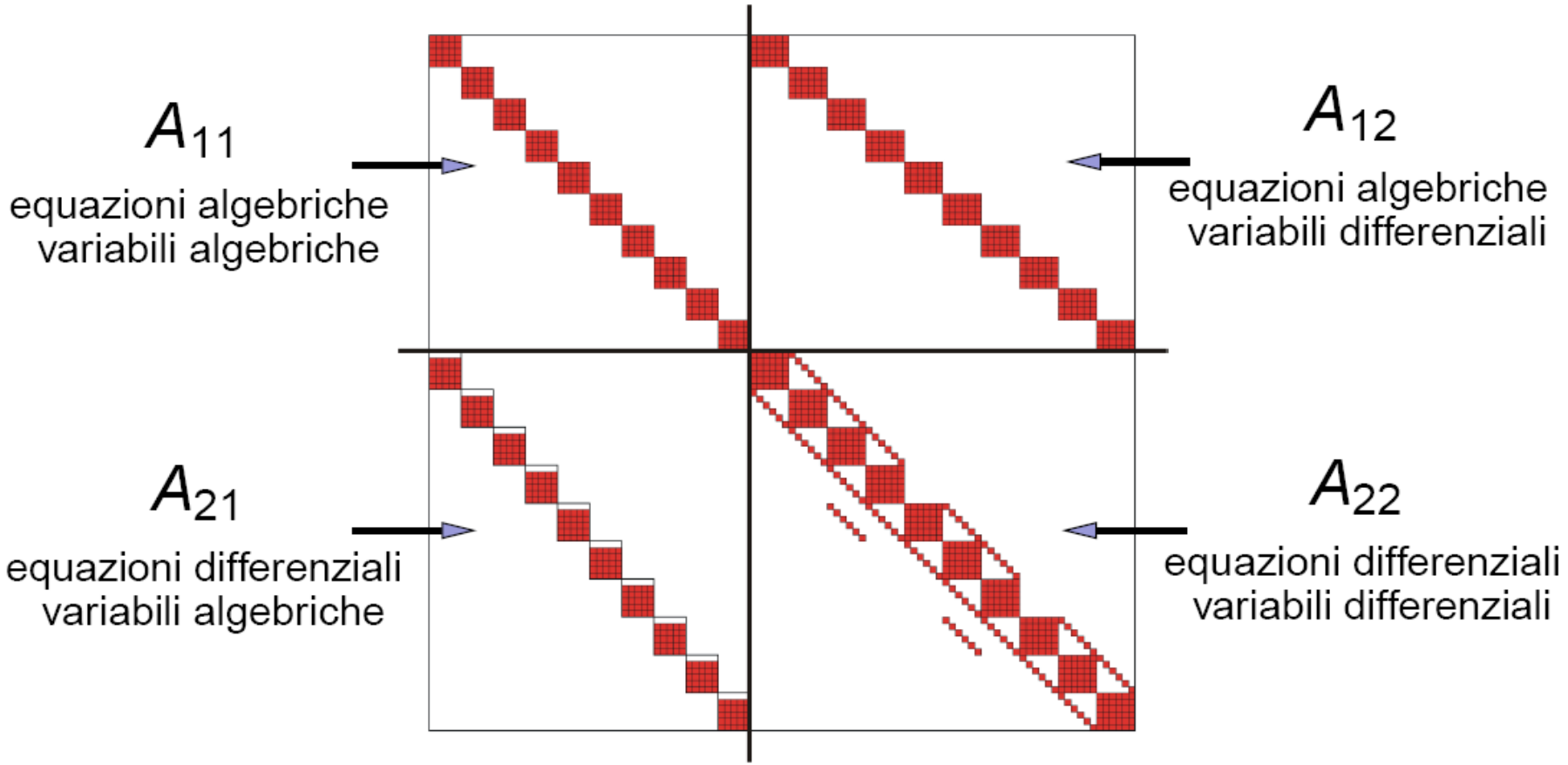

Risoluzione numerica sistema DAE

- Tempo simulazione: 4000 s
- Tempo di switch: 40 s
- Numero nodi discretizzazione spaziale: 97
- Numero totale equazioni per nodo: 11
- Numero totale DAE: 1067

- CPU: Intel® Pentium IV 2.4 GHz
- RAM: 512 MB
- OS: MS Windows XP Professional
- Compilatore: COMPAQ Visual Fortran 6.1
  + MICROSOFT C++ 6.0

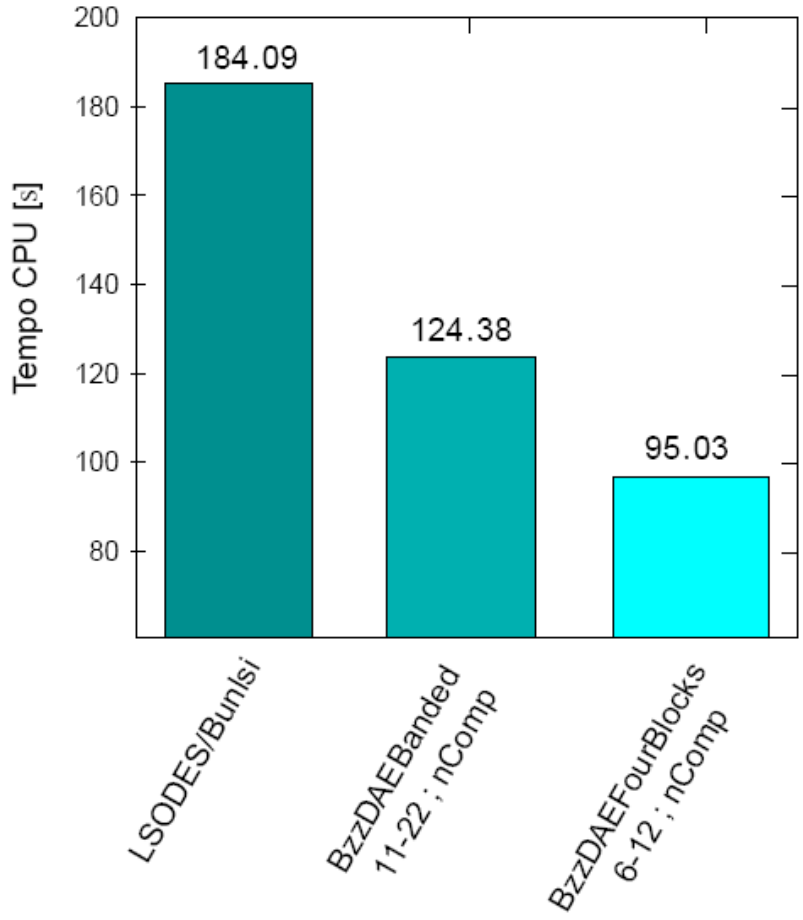

Numerical simulation

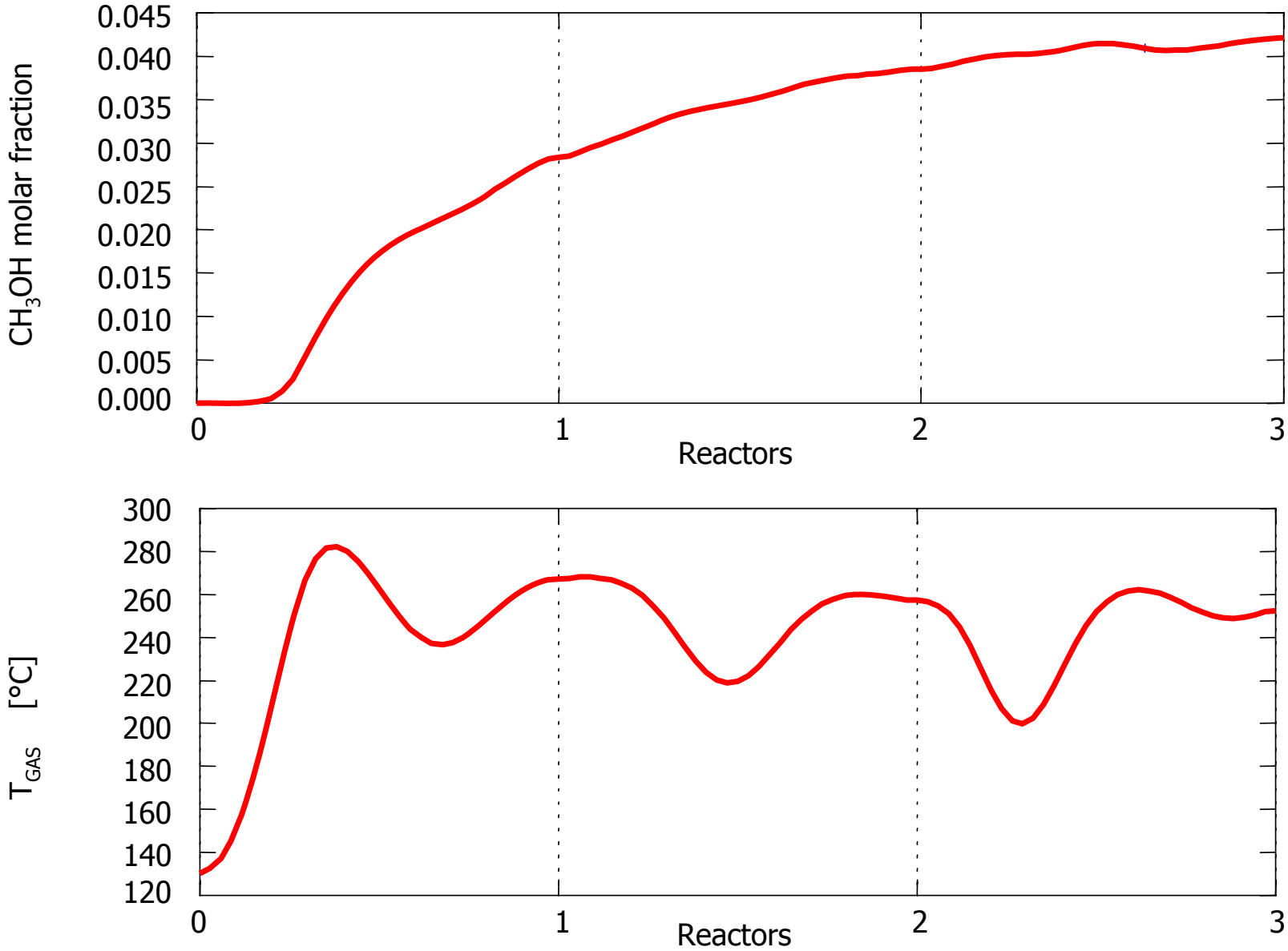

Numerical simulation

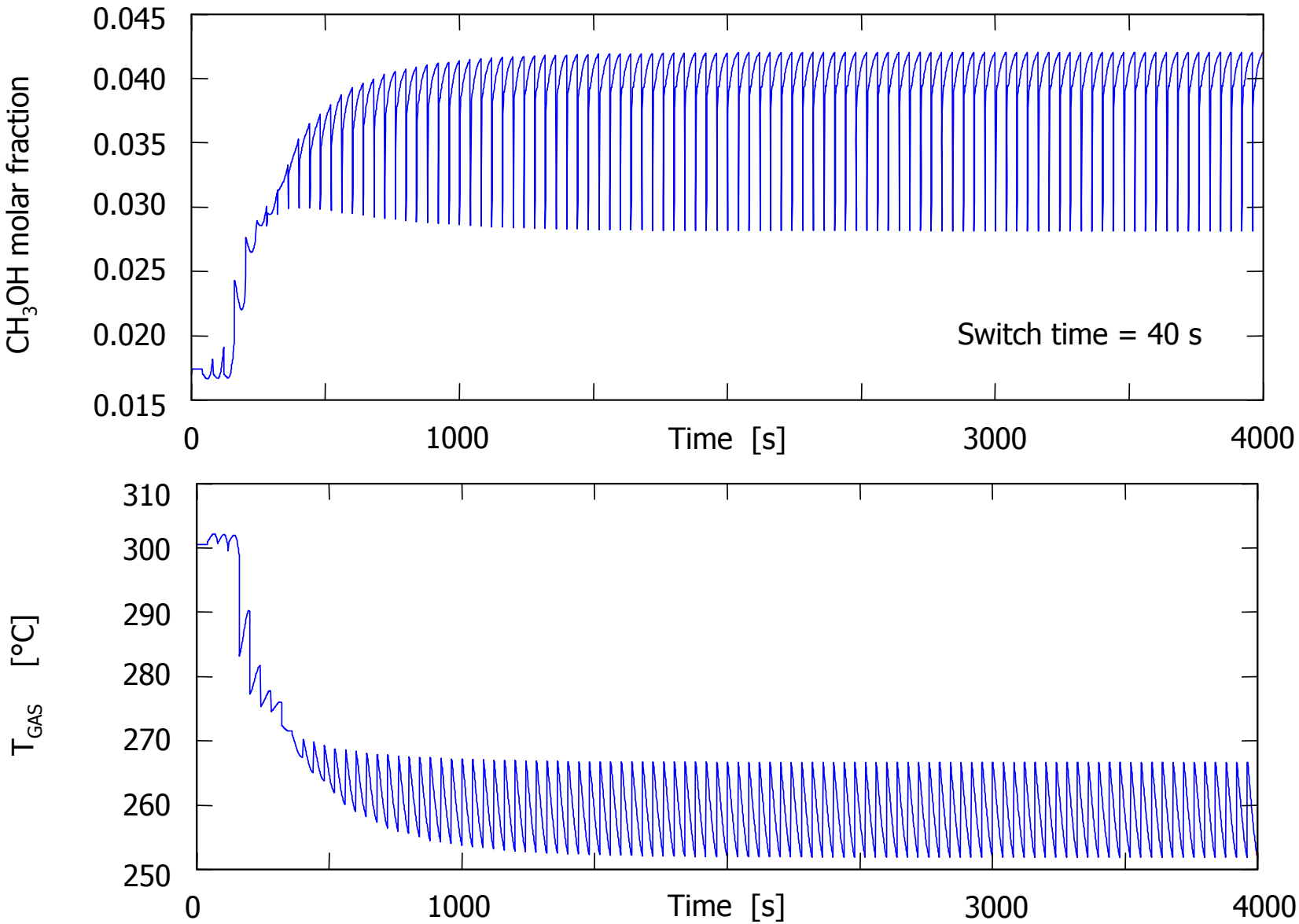

Studio di sensitività parametrica

- Grandezze analizzate e range di variabilità

Variabile	Intervallo
Temperatura gas in ingresso, T_{in} [K]	300÷593
Velocità gas in ingresso, v_{in} [m/s]	0.0189÷0.0231
Tempo di switch, t_c [s]	1÷350

Studio di sensitività parametrica

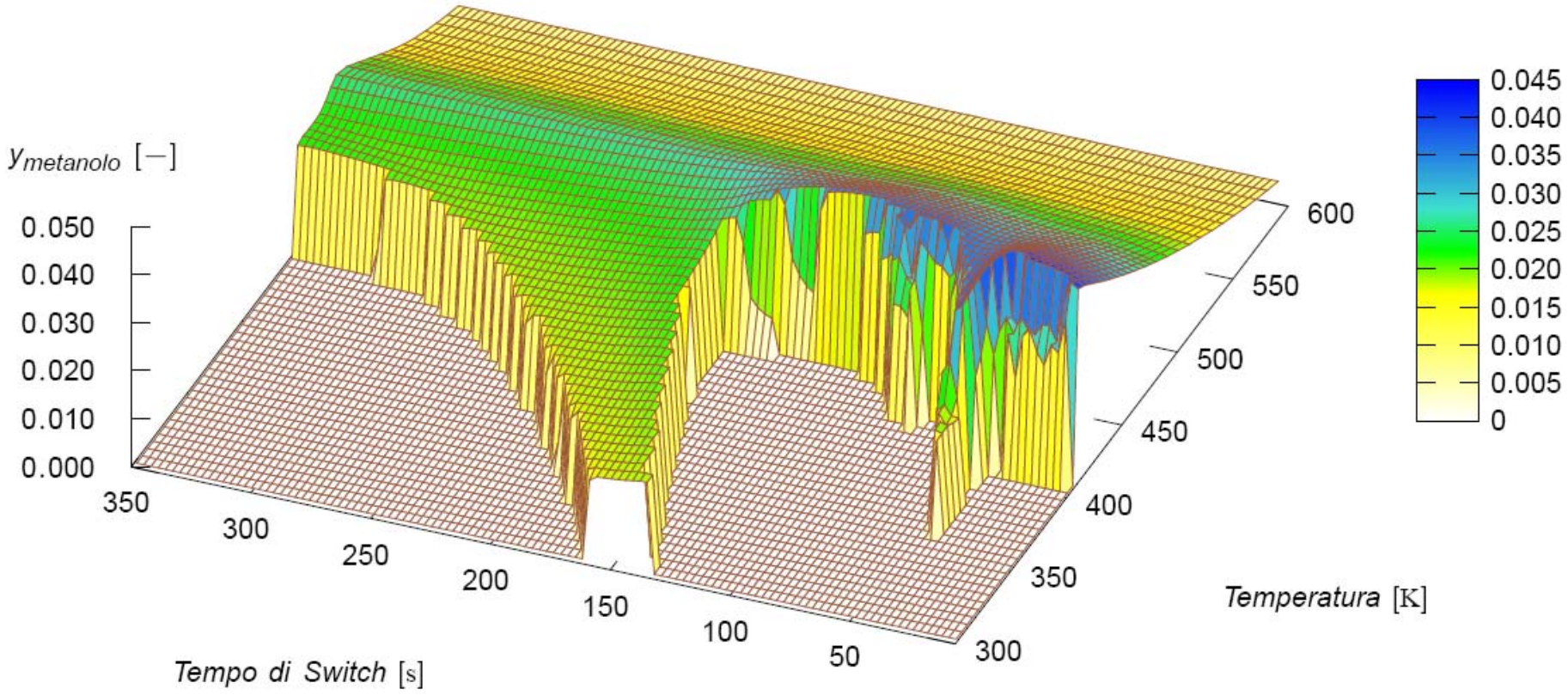

Studio di sensitività parametrica

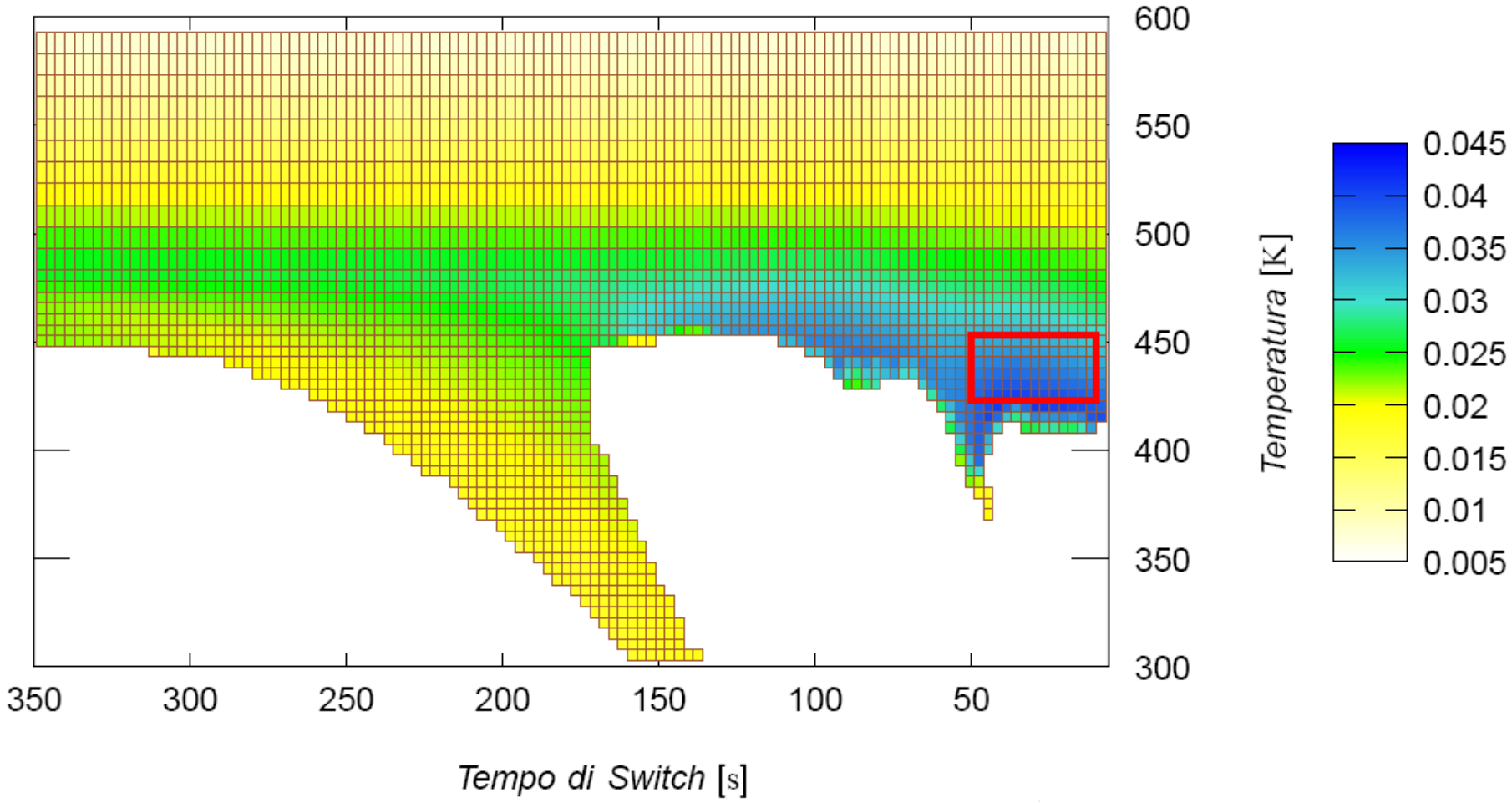

Studio di sensitività parametrica

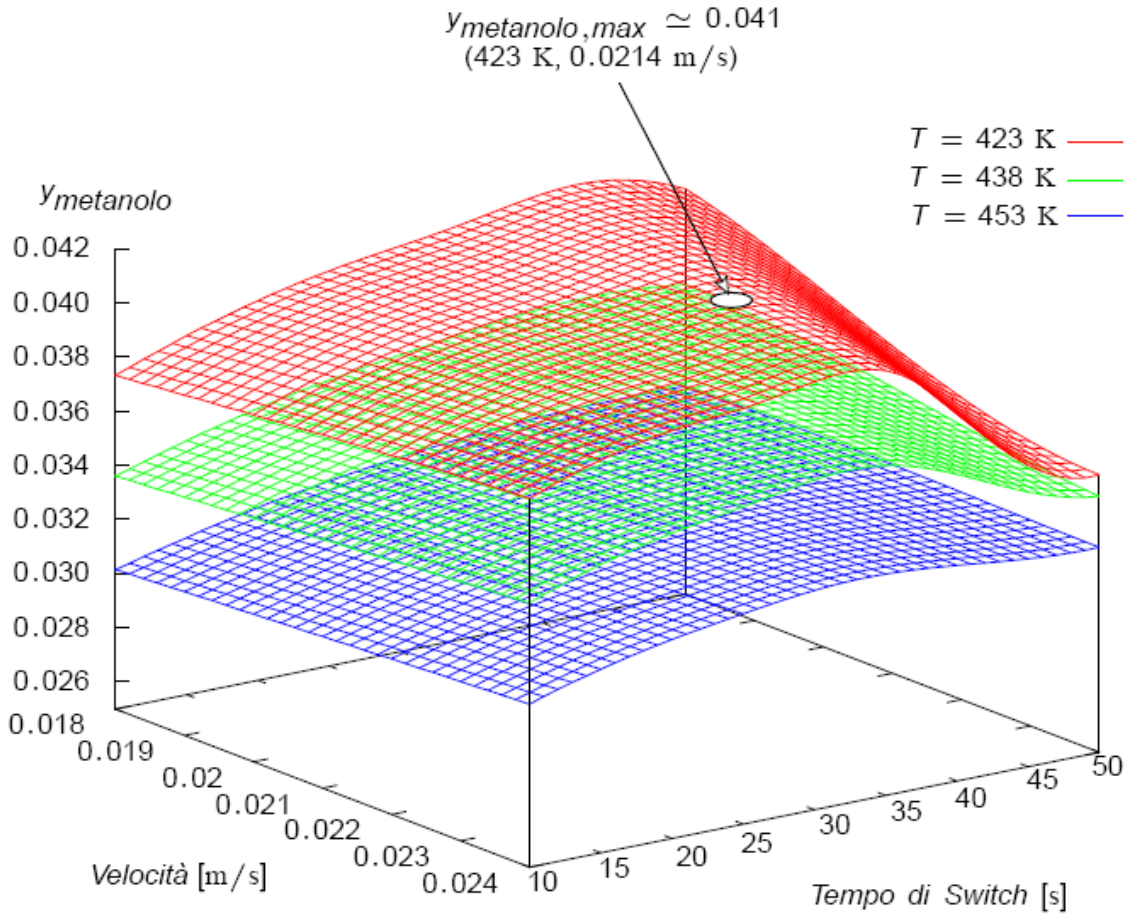

Need for speed

- **THE POINT**: to simulate 100 switches of the inlet flow with a switch time of 40 s (total of 4,000 s) the DAE system, comprising 1067 equations, takes about **95 s of CPU time** on a Pentium IV @ 2.4 GHz.

- **PROBLEM**: the detailed first principles model requires a CPU time that is prohibitive for model based control purposes.

- **SOLUTION**
  - A **high efficiency** numerical model in terms of CPU time is therefore required;
  - Such a model should be able to describe the **nonlinearities** and the articulate profiles of the network of reactors;
  - Artificial Neural Networks, **ANN**, may be the answer.

Identificazione di sistema tramite ANN

ANN architecture

Input variables	Range
Inlet gas temperature, T_{in} [K]	423÷453
Inlet gas velocity, v_{in} [m/s]	0.0189÷0.0231
Switch time, t_c [s]	10÷50

Output variables
Mean methanol molar fraction, x_{CH3OH}
Outlet gas temperature, T_{GAS} [K]

ANN architecture

Levels		# of nodes	Activation function
1	Input	40	Sigmoid
2	Intermediate 1	15	Sigmoid
3	Intermediate 2	15	Sigmoid
4	Output	1	Linear
# of weights and biases		840 + 31 = **871**	
Learning factor, α		0.716	
Momentum, β		0.366	
Linear activation constant, μ		0.275	

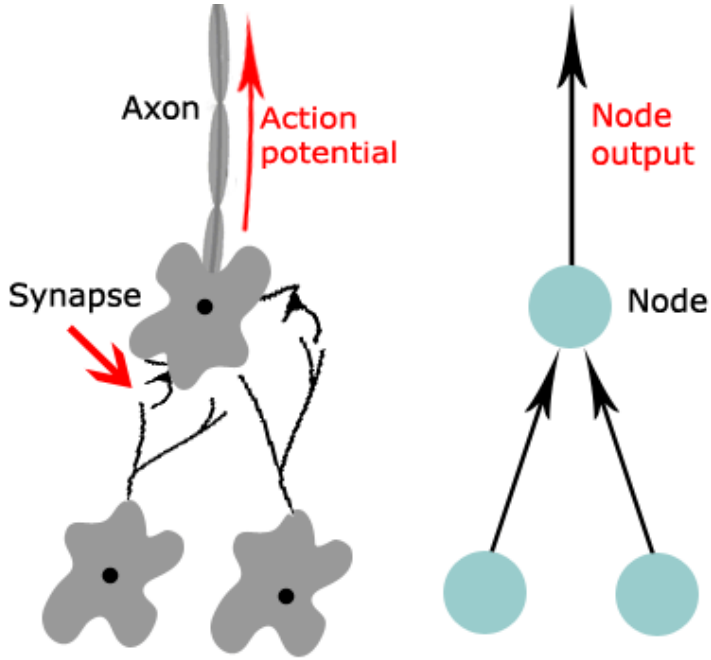

Random input patterns

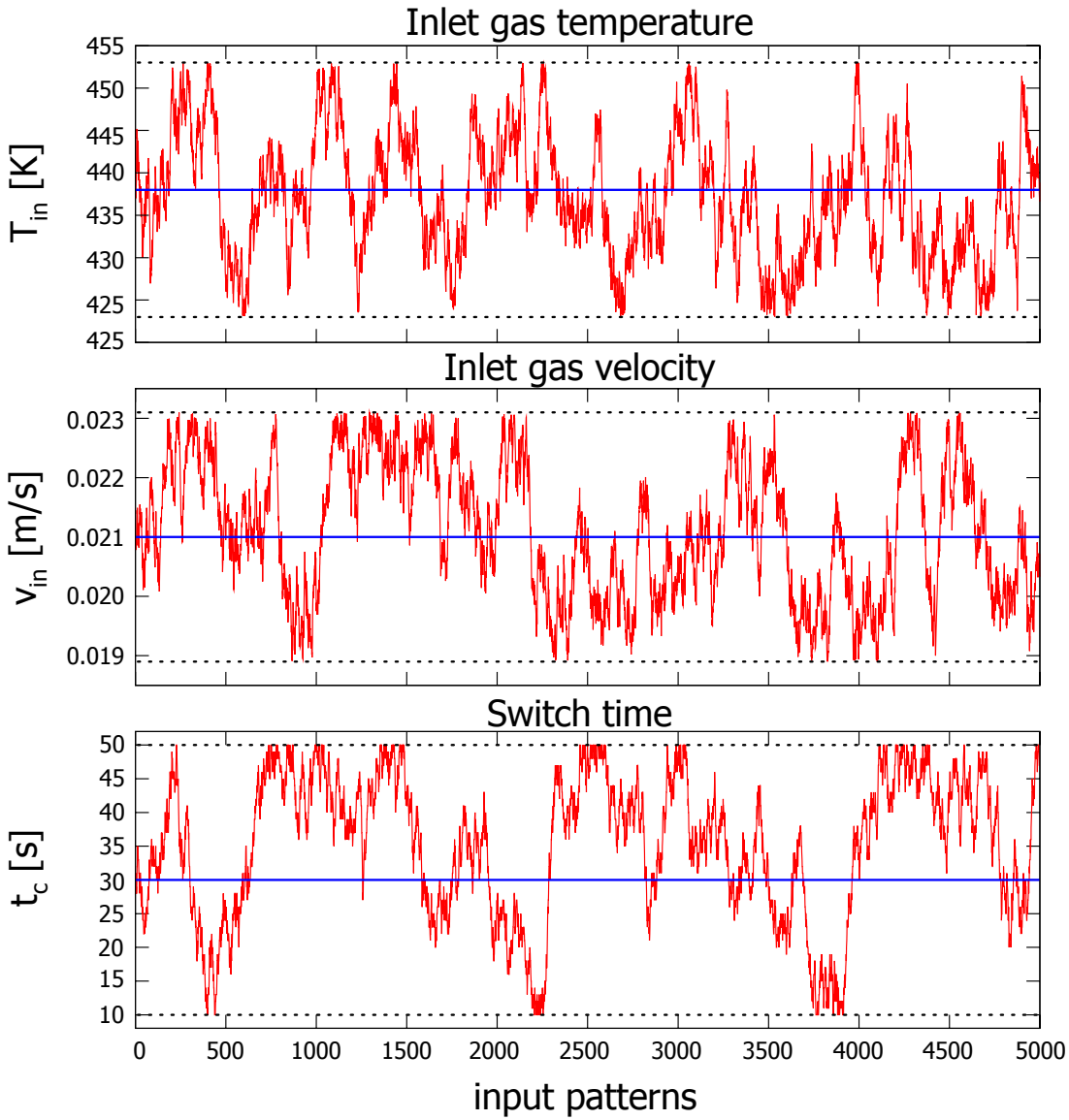

Levemberg Marquard learning algorithm

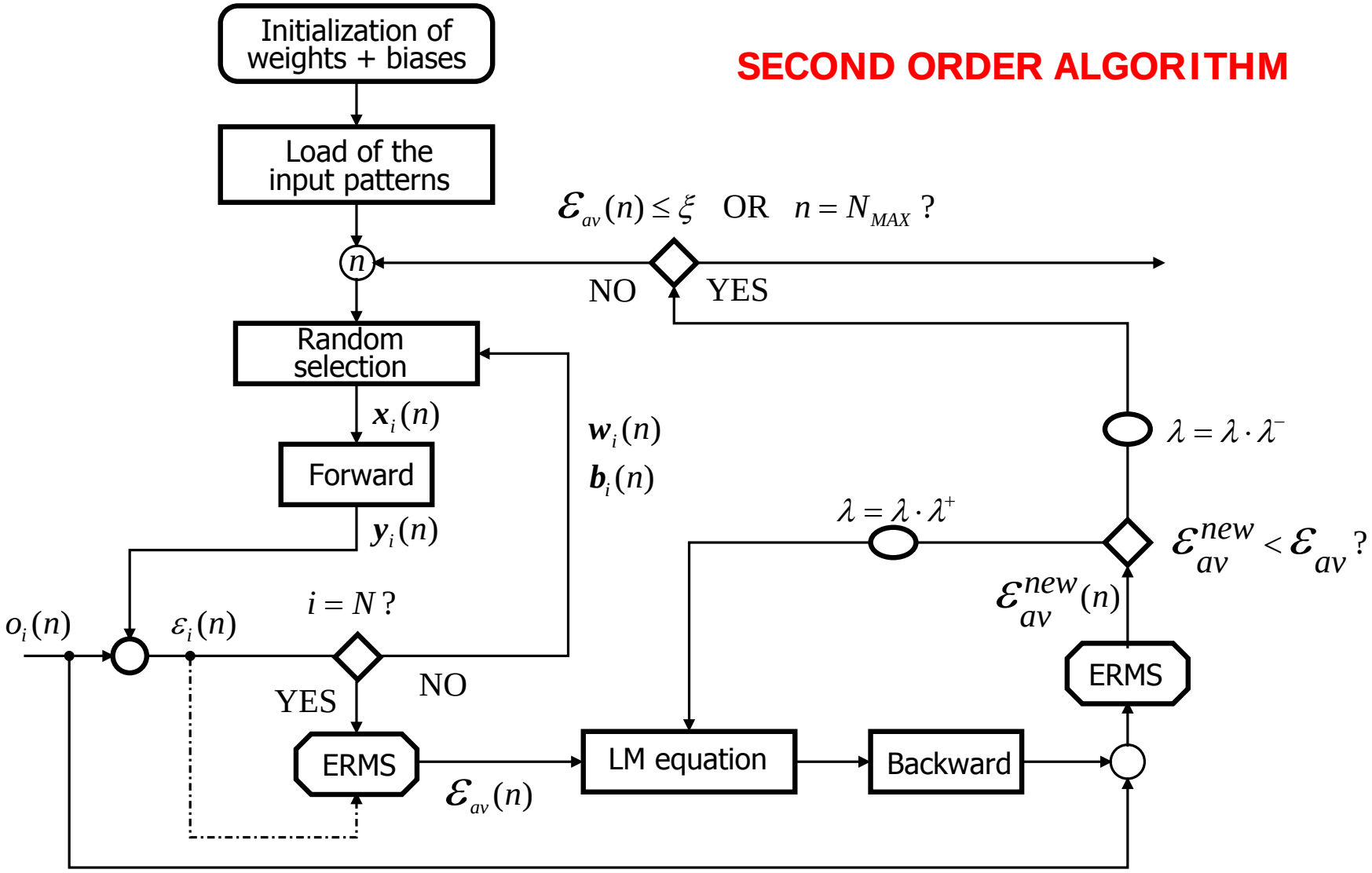

Comparing algorithms...

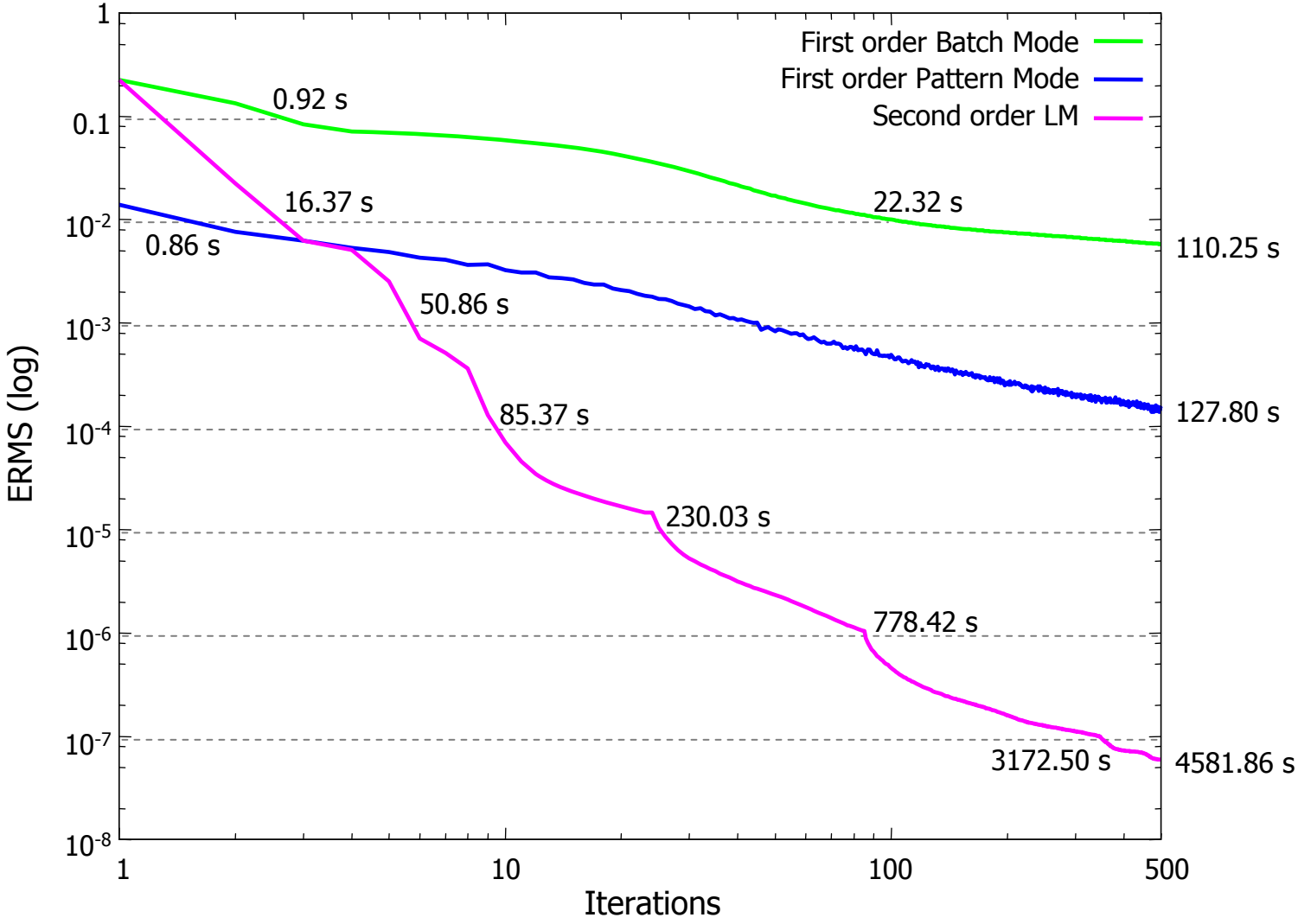

The overlearning problem

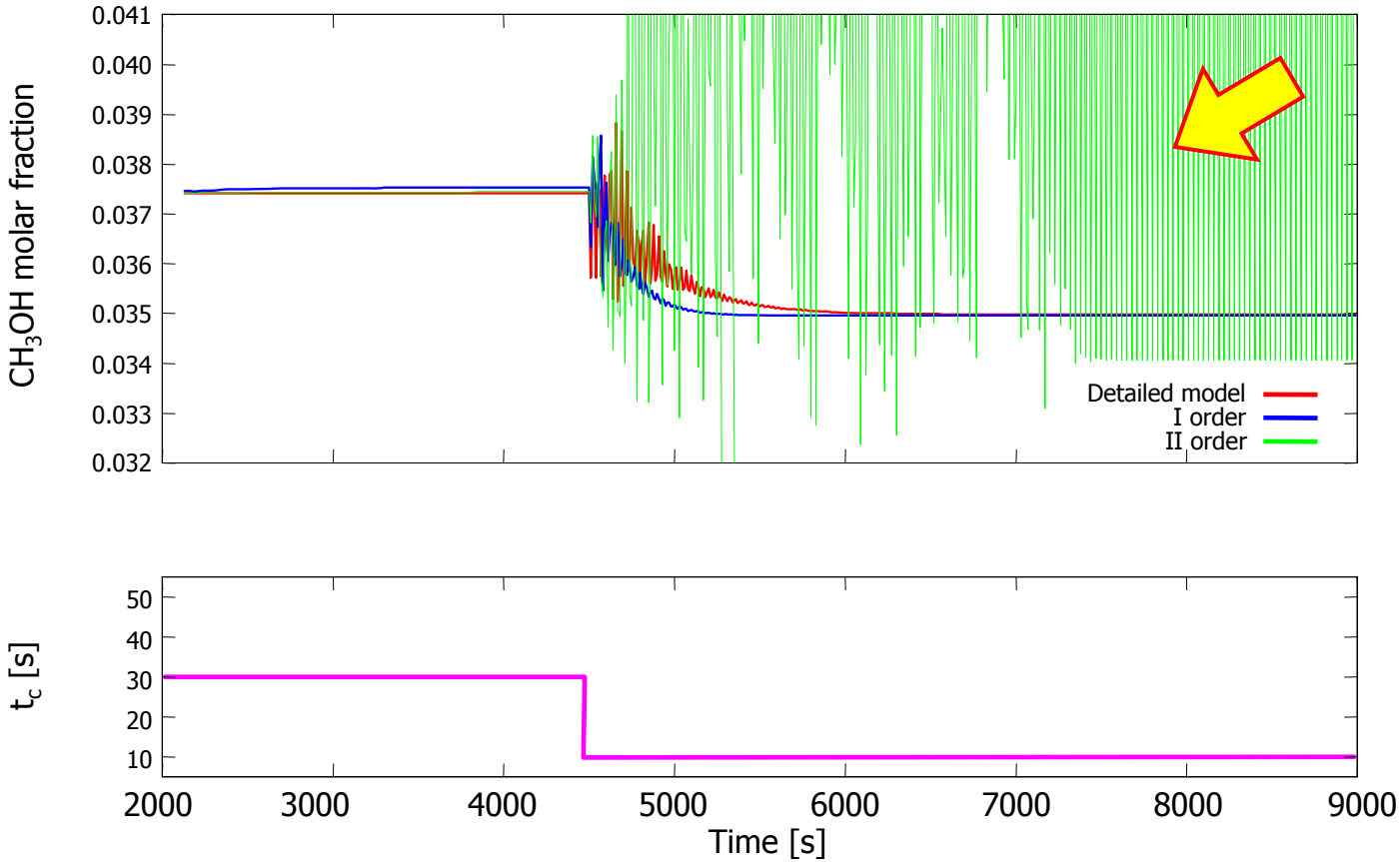

Disturbance on the **switch time** (from 30 to 10 s)

The overlearning problem

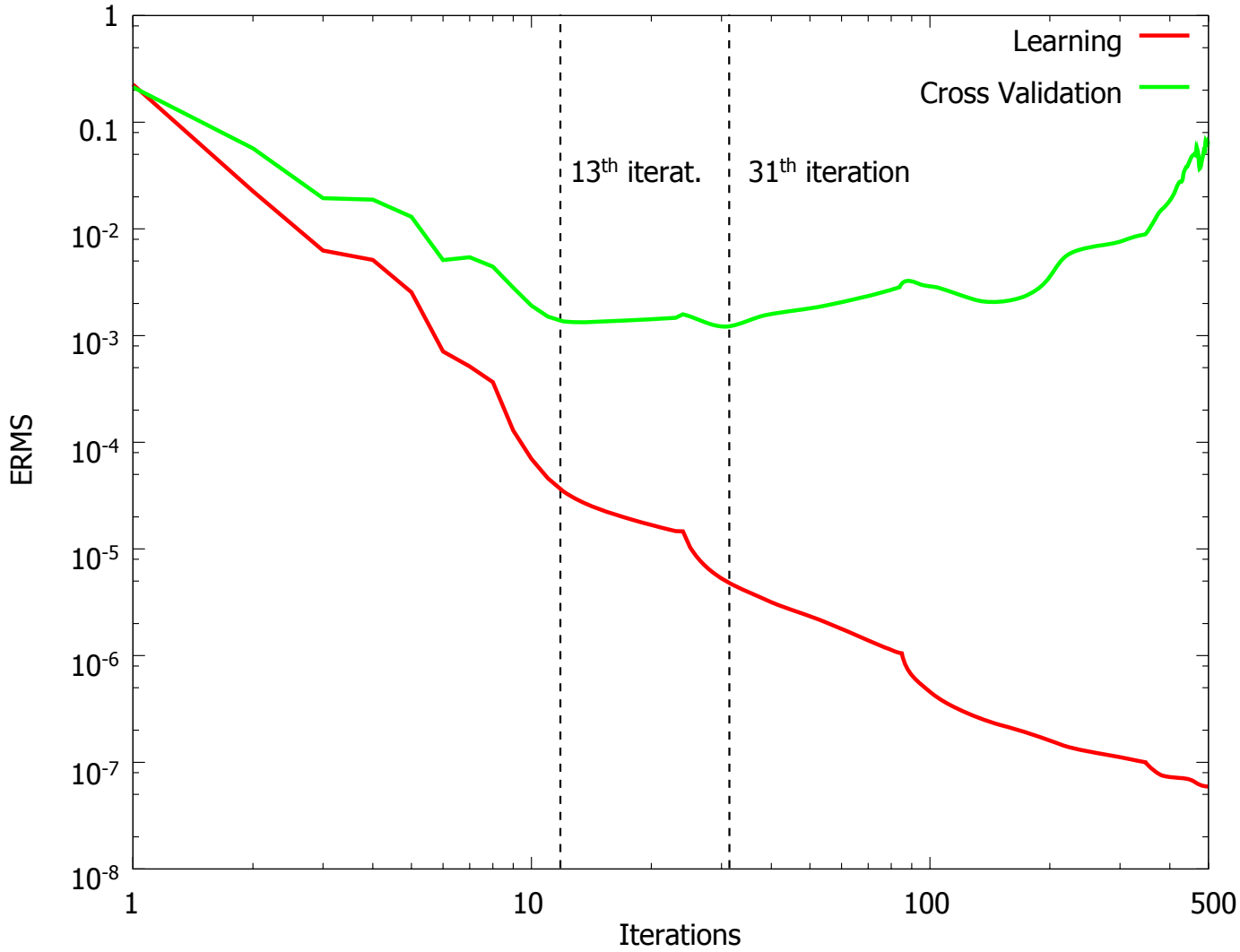

ANN cross-validation

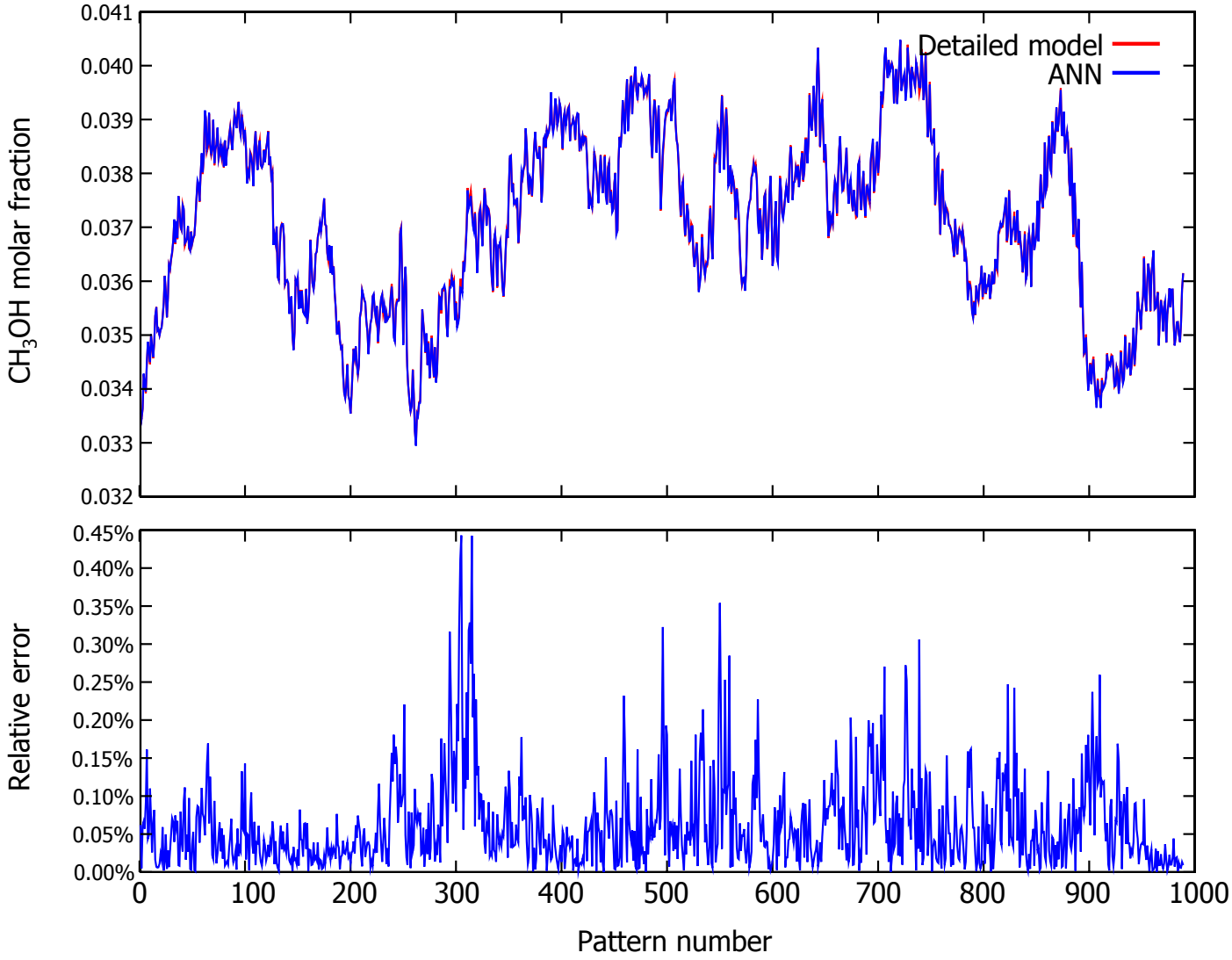

ANN disturbance response

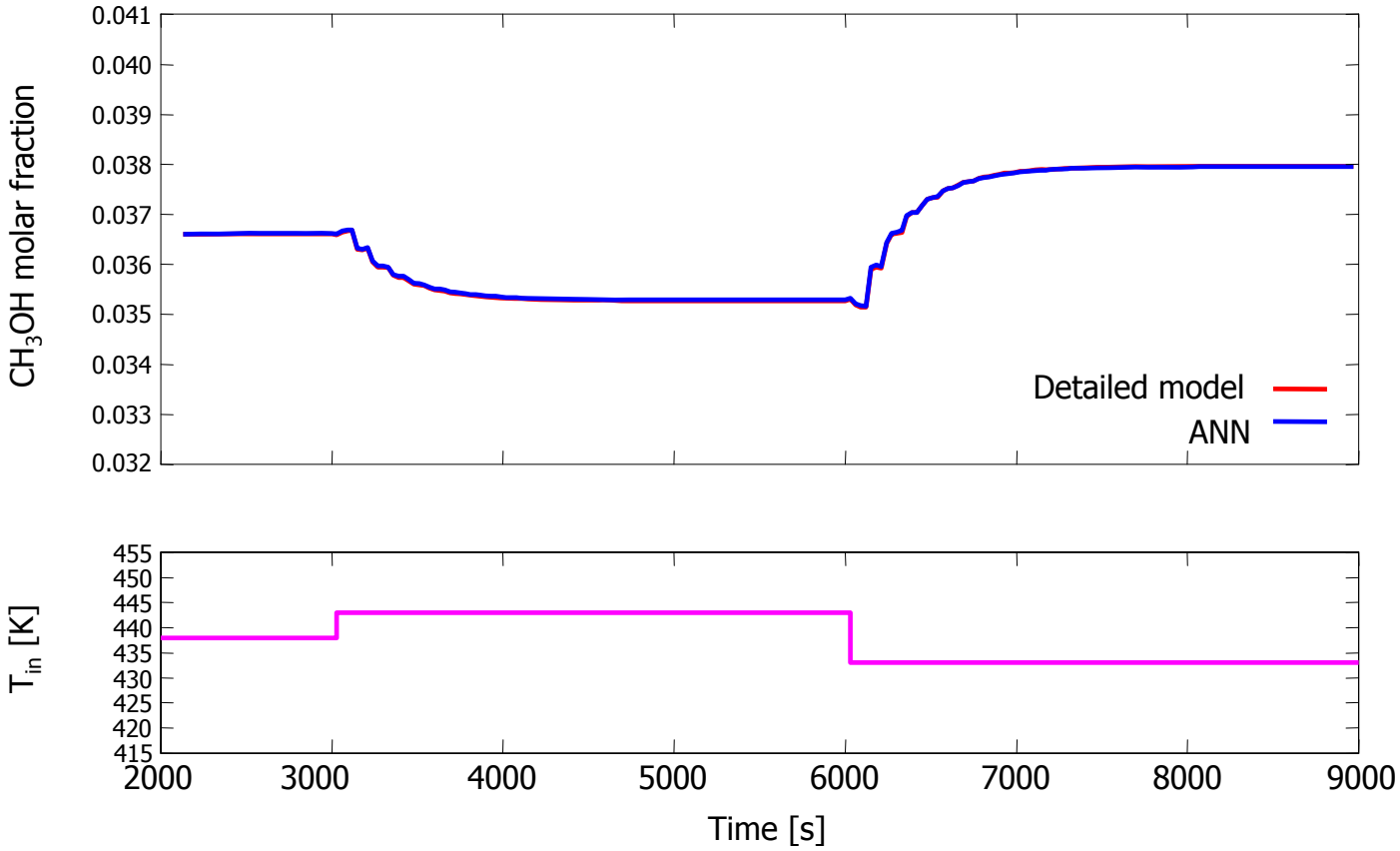

Disturbance on the **inlet temperature** 438 → 443 → 433 [K]

ANN disturbance response

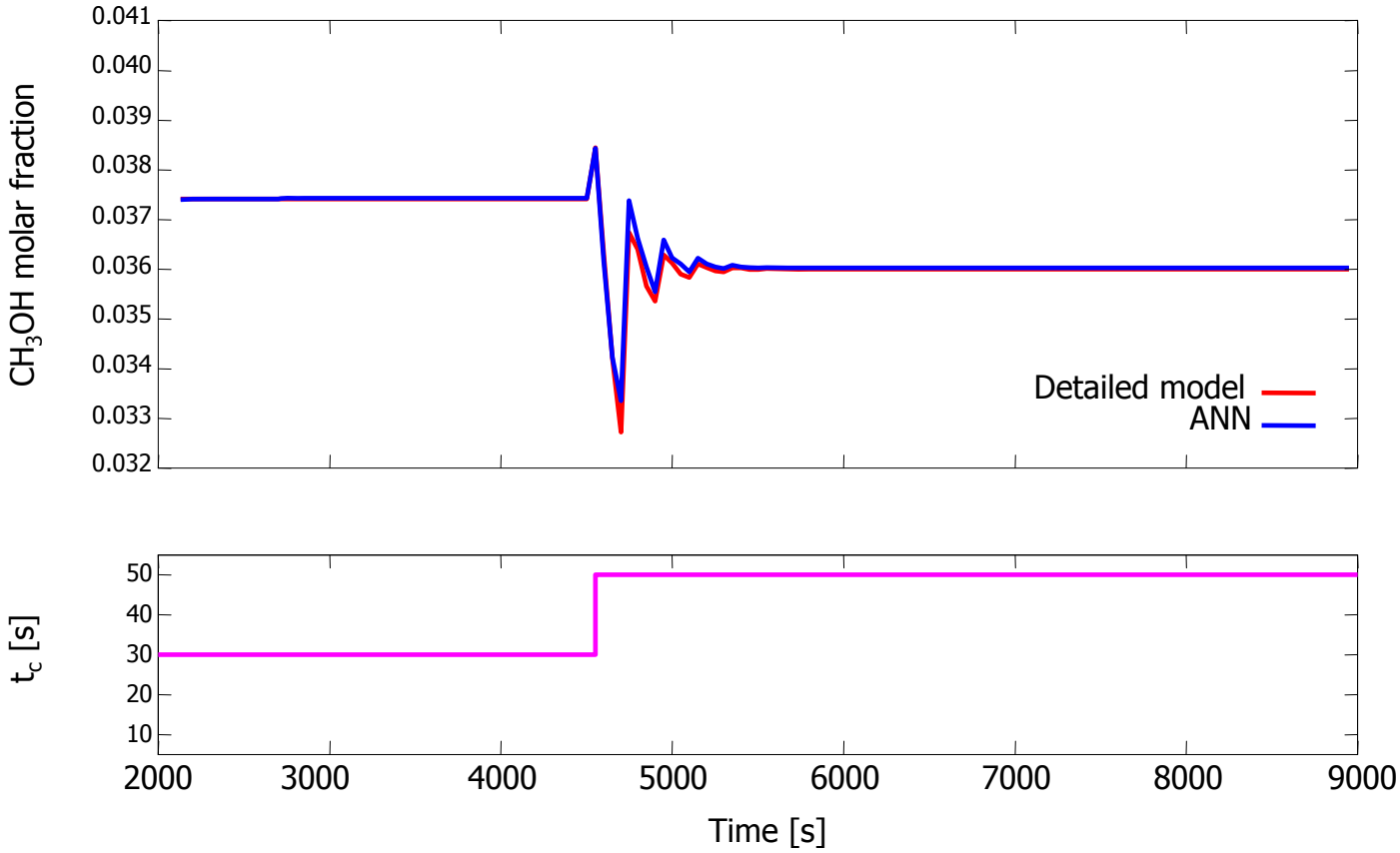

Disturbance on the **switch time** 30 → 45 [s]

ANN disturbance response

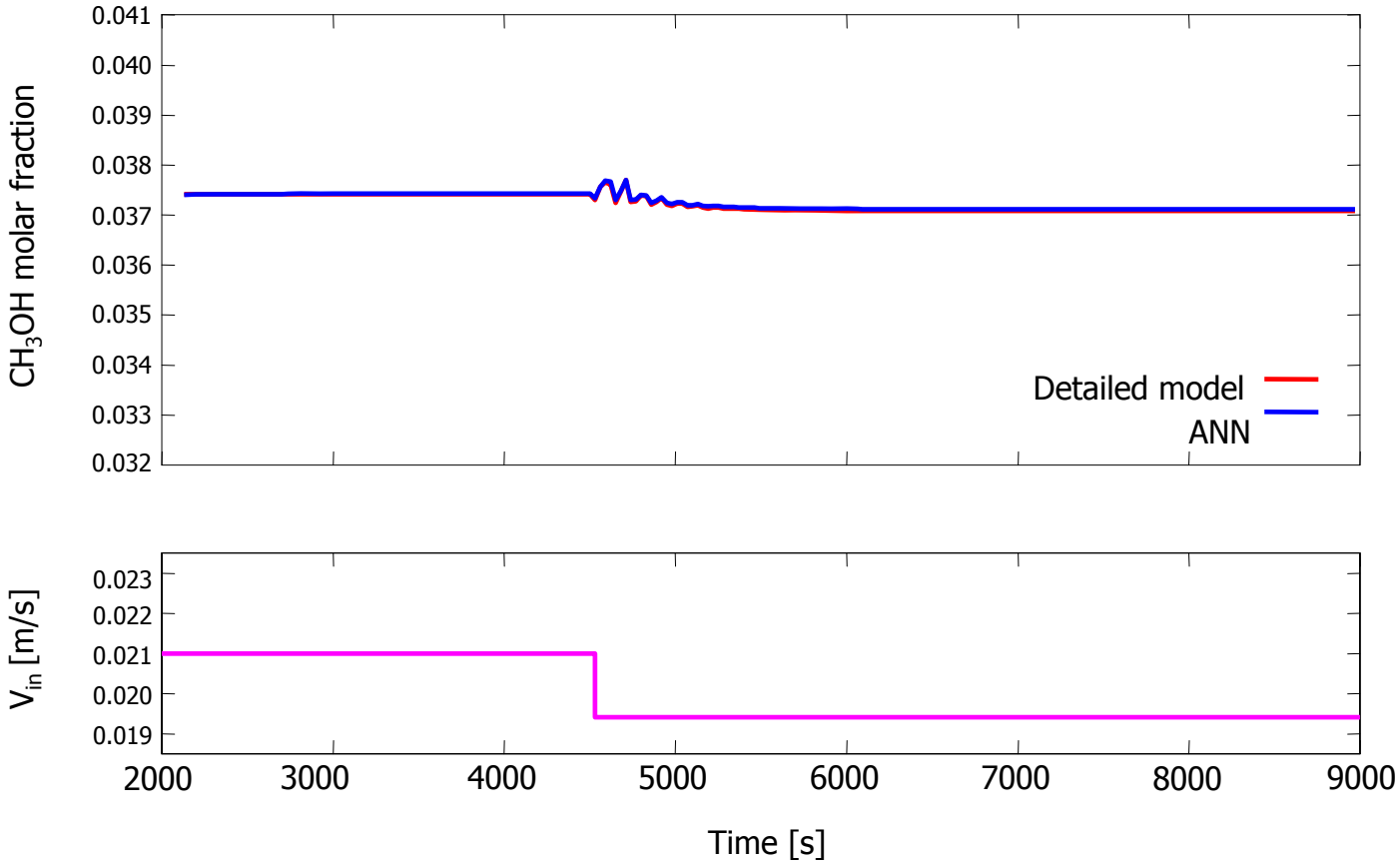

Disturbance on the **inlet velocity** 0.021 → 0.0194 [m/s]

ANN CPU times

	MISO		MIMO
ANN Output variables	CH_3OH	T_G	CH_3OH+T_{GAS}
# of output nodes	1	1	2

# of weights and biases	840+31=871	840+31=871	855+32=887
Jacobian matrix dimensions	4000 x 871	4000 x 871	8000 x 887
CPU time for evaluating J^TJ [s]	17.38	17.37	49.13
Learning procedure CPU time	3h 14 min	3h 13 min	8 h 18 min

CPU time for a **single ANN simulation** [s]	**8.08E-6**	**8.23E-6**	**8.86E-6**

ABOUT 6 ORDERS OF MAGNITUDE IMPROVEMENT BETWEEN THE FIRST PRINCIPLES MODEL AND THE ANN

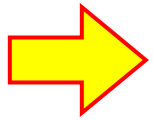

ON-LINE FEASIBILITY OF MODEL BASED CONTROL